Generalized q-Analysis of Log-Periodicity: Applications to Critical Ruptures

Wei-Xing Zhou [1] and Didier Sornette [1,2,3]

1. Institute of Geophysics and Planetary Physics, University of California, Los Angeles, CA 90095
2. Department of Earth and Space Sciences, University of California, Los Angeles, CA 90095
3. Laboratoire de Physique de la Matière Condensée, CNRS UMR 6622 and Université de Nice-Sophia Antipolis, 06108 Nice Cedex 2, France

Abstract

We introduce a generalization of the q-analysis, which provides a novel non-parametric tool for the description and detection of log-periodic structures associated with discrete scale invariance. We use this generalized q analysis to construct a signature called the (H, q)-derivative of discrete scale invariance, which we use to detect the log-periodicity in the energy release rate and its cumulative preceding the rupture of five pressure tanks made of composite carbon-matrix material. We investigate the significance level of the spectral Lomb periodogram of the optimal (H, q)-derivative. We confirm and strengthen previous parametric results that the energy release rate and it cumulative exhibit log-periodicity before rupture. However, our tests to use this method as a scheme for the prediction of the critical value of the stress at rupture are not encouraging.

1 Introduction

The fracture of materials is a catastrophic phenomenon of considerable technological and scientific importance. However, a reliable identification of precursory signatures of impending failure is lacking in most cases. A notable exception has been found [1, 2] in the analysis of acoustic emissions recorded during the pressurization of spherical tanks of kevlar or carbon fibers pre-impregnated in a resin matrix wrapped up around a thin metallic liner (steel or titanium) fabricated and instrumented by Aérospatiale-Matra Inc. (now EADS). A recent thorough analysis [3] of the seven acoustic emission recordings of seven pressure tanks, that was brought to rupture, has unambiguously characterized the acceleration of acoustic energy rate dE/dt and found it to be in agreement with a power law "divergence" expected from the critical point theory proposed in Ref. [4]. In addition, strong evidence of log-periodic corrections was found [3], that quantify the intermittent succession of accelerating bursts and quiescent phases of the acoustic emissions on the approach to rupture. Ref. [3] also proposed an improved model accounting for the cross-over from the non-critical to the critical region close to the rupture point exhibits interesting predictive potential. The critical rupture concept, confirmed by other experiments [5], opens the road towards industrial applications involving heterogeneous materials such as fiber composites, rocks, concrete under compression and materials with large distributed residual stresses [6].

However, a time-to-failure behavior following a power law $dE/dt \propto (t_c - t)^{-\alpha}$ does not provide a reliable and unique signature: fits of noisy data by such power laws are notoriously unreliable; for instance, an error of 1% in the determination of t_c usually leads to errors of tens of percent for the exponent α. In addition, the determination of t_c is very sensitive to the presence of noise. In order

to improve the determination of t_c, the existence of log-periodic oscillations have been found useful [1, 7, 8] and have been used for the implementation of prediction schemes [1, 2, 3] with reasonable success.

The demonstration of the existence of log-periodic corrections to the power law is of both fundamental and practical interest. From a fundamental point of view, log-periodicity signals a spontaneous hierarchical organization of damage with an approximate geometrical set of characteristic scales. A possible mechanism involves a succession of ultraviolet instabilities of the Mullins-Sekerka type [9] (see also [10] for a review). More generally, the presence of log-periodicity signals the partial breaking of continuous scale invariance into discrete scale invariance, which requires that the underlying field theory be non-unitary [11]. From a practical view point, log-periodicity may help locking in the fit on experimental data to obtain a better precision on the recovery of the critical rupture time t_c [1, 2, 3].

However, most of the evidence of log-periodicity in rupture results from parametric fits of the experimental or numerical data by a log-periodic power law formula, except for Ref. [7] which introduced a "canonical" averaging method to extract the log-periodic signal directly. Parametric fits suffer from two problems: (1) the formula cannot avoid some simplification which for instance omits the presence of harmonics and/or other structures; (2) parametric fits are delicate due to possible degeneracies and, in addition, their statistical significance (i.e., added value) is difficult to estimate. It is thus important to develop further non-parametric tests. This is our goal here to present a novel non-parametric method, that turns out to be very powerful in identifying log-periodicity in noisy data.

Our method is based on the concept of a q-derivative, the inverse of the Jackson q-integral [12], which is the natural tool [13, 14] for describing discrete scale invariance. Indeed, q-derivatives can be identified with the generators of fractal and multifractal sets with discrete dilatation symmetries [14]. Nowhere differentiable functions which characterize fractal or multifractal sets turn out to be perfectly well behaved under the q-derivative. Discrete renormalization group equations, whose general mathematical solutions are power laws with complex exponents (and hence exhibit log-periodicity), can be seen as nothing but Jackson q-integrals of regular functions of the decimated degrees of freedom. Jackson q-integrals constitutes the natural generalization of regular integrals for discretely self-similar systems [14]. The way that Jackson q-integral can be related to the free energy of a spin system on a hierarchical lattice was explained in [13].

In section 2, we introduce the q-derivative and generalize it to take into account of anomalous scaling. We discuss the main properties of the generalized q-derivative that will be useful for our analysis of this paper. Section 3 presents our analysis with the generalized q-derivative of the acoustic emission data, both for the energy release rate and for the cumulative energy release, obtained during the pressurization of spherical tanks of kevlar or carbon fibers pre-impregnated in a resin matrix wrapped up around a thin metallic liner (steel or titanium). For comparison, we use exactly the same set of seven acoustic emission recordings of the seven pressure tanks used in the previous study reported in [3]. Our new results confirm strongly the existence of log-periodicity with a much enhanced confidence. Section 4 tests a scheme using the generalized q-derivative for prediction purpose. Here, we find disappointing results: the parametric approach in [3] turns out to be more powerful.

2 The generalized q-analysis and log-periodicity

2.1 Definition

Let us take some $q \in (0,1) \cup (1,\infty)$. The q-derivative of an arbitrary function $f(x)$ is defined as

$$D_q f(x) = \frac{f(x) - f(qx)}{(1-q)x} \ . \tag{1}$$

For $q \to 1$, the definition (1) recovers the usual definition of a derivative.

For $q \neq 1$, $D_q f(x)$ is more than just a derivative: it compares the relative variations of $f(x)$ and of x when x is magnified by the finite factor q. It is thus intuitive that the q-derivative tests the scale invariance property of the function $f(x)$. As we said above, it was actually shown by Erzan and Eckmann [14] that the q-derivative is the natural tool for describing discrete scale invariance, since a fixed finite q compares $f(x)$ with $f(qx)$ at x magnified by a fixed factor, and thus it also compares $f(qx)$ with $f(q^2x)$, $f(q^2x)$ with $f(q^3x)$, etc. When x is taken as the distance from a critical point, $D_q f(x)$ thus quantifies the discrete self-similarity of the function $f(x)$ in the vicinity of the critical point. From the definition (1), it is clear that

$$D_{1/q} f(x) = D_q f(x/q) \ . \tag{2}$$

It is thus enough to study $D_q f(x)$ for $q \in (0,1)$ to derive its values for all q's.

The necessary and sufficient condition for a function $f(x)$ of order ψ to be homogeneous is

$$D_q f(x) = \frac{q^\psi - 1}{q-1} \frac{f(x)}{x} \ . \tag{3}$$

This expression suggests the introduction of a generalized q-derivative that we call (H,q)-derivative, such that the dependence in x of $D_q^H f(x)$ disappears for homogeneous functions, for the choice $H = \psi$. Consider therefore the following definition

$$D_q^H f(x) \triangleq \frac{f(x) - f(qx)}{[(1-q)x]^H} \ , \tag{4}$$

such that $D_q^{H=1} f(x)$ recovers the standard q-derivative $D_q f(x)$. For a power law function $f(x) = Bx^m$, $D_q^{H=m}[Bx^m] = B(1-q^m)/(1-q)^m$ is constant. For a statistically homogeneous function $f(x) \stackrel{d}{=} Bx^m$, $D_q^{H=1} f(x) \stackrel{d}{=}$ constant.

The generalized (H,q)-derivative has two control parameters: the discrete scale factor q devised to characterize the log-periodic structure and the exponent H introduced to account for a possible power law dependence, i.e., to trends in log-log plots.

2.2 Application to log-periodic functions

Since Erzan and Eckmann [14] showed that the q-derivative is the natural tool for describing discrete scale invariance, it is natural to study the properties of the (H,q)-derivative of the simplest function exhibiting discrete scale invariance, namely a power law decorated by a simple log-periodic function:

$$y(x) = A - B\tau^m x^m + C\tau^m x^m \cos(\omega \ln x) \ , \tag{5}$$

where the presence of a phase $\phi = \omega \ln \tau$ has been absorbed in the definition of x, $0 < C < B$ and $\omega = 2\pi f$. This equation, where x is interpreted as the normalized distance $x = (p_c - p)/\tau$ to a critical point p_c, has been used in several works to describe material rupture [1, 2, 8, 3], precursory patterns of large earthquakes [15], rock bursts [16], aftershocks [17, 18], and speculative bubbles preceding financial crashes [19].

The (H,q)-derivative of $y(x)$ is

$$D_q^H y(x) = x^{m-H}[B' + C' g(x)] \,, \tag{6}$$

where

$$B' = -\frac{B\tau^m(1-q^m)}{(1-q)^H}, \qquad C' = \frac{C\tau^m}{(1-q)^H} \tag{7}$$

and

$$g(x) = C_1 \cos(\omega \ln x) + C_2 \sin(\omega \ln x) \,, \tag{8}$$

with $C_1 = 1 - q^m \cos(\omega \ln q) > 0$ and $C_2 = \sin(\omega \ln q)$. The special choice $H = m$ gets rid of the power law and the (H,q)-derivative $D_q^H y(x)$ becomes the pure log-periodic function $g(x)$.

For the special choices $q = e^{-n2\pi/\omega}$ where n is a positive integer corresponding to choosing q equal to one of the preferred scaling factor of the log-periodic function, we obtain $C_1 = 1 - q^m$ and $C_2 = 0$. Therefore, the (H,q)-derivative offers a novel approach for detecting the preferred scaling factors of the discretely scale invariant function by a measure of its phase: those values of q such that the phases of the $(H = m, q)$-derivative is that of a pure cosine should qualify as the preferred scaling factors. Such phases can be for instance measured by the Hilbert transform. Here, we do not persue this possibility which wll be explored in another presentation.

In the Appendix A, it is shown that $g(x)$ is extremal at x_m solution of

$$\omega \ln(x_m) = n\pi + \arctan(C_2/C_1) \,, \tag{9}$$

where $n = 0, \pm 1, \pm 2, \cdots$, and that the extreme values of $g(x)$ are

$$g(x_m) = \pm\sqrt{C_1^2 + C_2^2} \,. \tag{10}$$

The amplitude of $D_q^H y(x)$ is then

$$A = x_m^{m-H}\ C' \sqrt{C_1^2 + C_2^2} \,, \tag{11}$$

while the successive extreme values are

$$D_m = \left(B' \pm C'\sqrt{C_1^2 + C_2^2}\right)(x_m)^{m-H} \,, \tag{12}$$

where B' and C' are defined in (7). By fixing H close to m, one can in principle obtain the amplitude A_m to be constant as a function of x. This value $H = m$ should provide theoretically the most significant log-periodic component, quantified for instance by the largest peak of the Lomb periodogram. However, in practice, the noise embedded in the data may distort the log-periodic oscillations and the most significant log-periodicity may occur for $H \neq m$. The introduction of H affords a convenient detrending scheme.

Figure 1 shows $y(x)$ defined in Eq. (5) as a function of the distance x to the critical point with $A = 1260$, $B = 300$, $C = 6$, $m = 0.3$, $\omega = 5.4$ and $\phi = 0$. Figure 2 shows its generalized q-derivative with $q = 0.5$ for $H = 0.2$, $H = 0.3$ and $H = 0.4$, respectively. This generalized q-derivative has been calculated by using the incorrect assumption that the critical point is at $x = 1$ in order to also show the distortion resulting from an error in the determination of the critical point. This distortion becomes important when x is not large compared to 1. We observe that the amplitude of the oscillations of $D_q^H y(x)$ increases with H when going towards the critical point $x = 0$, in agreement with the prediction (11).

In the next section, using the (H,q)-analysis, we test for the presence of log-periodicity in the energy release rate and its cumulative obtained in the experimental recordings of the seven pressure tanks used in the previous study reported in [3].

3 Investigation of the significance of log-periodicity in acoustic emission energy release using the generalized (H, q)-analysis

We use the same notations to label the data sets as used in Ref. [3]. In this analysis, we use the true value p_c of the pressure at which rupture occurred in order to define the pressure-to-failure $p_c - p$ quantifying the distance to the critical rupture point. We follow [3] and use the acoustic emission data from the pressure at which a noticeable acceleration in the cumulative energy release takes place. This choice is not crucial at all, since the (H, q)-analysis is not sensitive to the points far from the critical point. We also exclude the last six points nearest to p_c because they contain the largest noise and may suffer from finite size effects that may lead to serious distortions. In our analysis, we exclude data sets of pressure tanks $\#\,5$ and $\#\,7$, because for these two data sets, $p_{\texttt{last}} \ll p_c$ (the last data point is for a pressure far below the critical rupture value). This leads to few oscillations and low statistical significance. We thus are left to analyze five data sets $\#\,1$, $\#\,2$, $\#\,3$, $\#\,4$ and $\#\,6$.

3.1 Energy release rate

In each analysis, q ranges from 0.1 to 0.9 with spacing 0.1, while H takes values from -0.9 to 0.9 with spacing 0.1. This defines $9 \times 19 = 171$ parameter pairs (H, q). For each parameter pair (H, q), we calculate the generalized q-derivative of the energy release rate. We then perform a spectral analysis of the generalized q-derivative using the Lomb periodogram method [20], in order to test for the statistical significance of possible log-periodic oscillations. For each (H, q) pair, the highest peak $P_N(H, q)$ and its associated logarithmic angular frequency $\omega(H, q)$ in the Lomb periodogram are obtained. The **first criterion** used to identify a log-periodic signal is the strength of the Lomb periodogram analysis, i.e., the height of the spectral peaks.

The results for the five data sets $\#\,1$, $\#\,2$, $\#\,3$, $\#\,4$ and $\#\,6$ are shown in Figs. 3 to 22. Figures 4, 8, 12, 16 and 20 show the dependence of the highest peak $P_N(H, q)$ in each Lomb periodogram as a function of H and q. Figs. 3, 7, 11, 15 and 19 give the associated logarithmic angular frequencies $\omega(H, q)$. The other figures show the generalized q-derivative for the pair (H, q) giving the highest Lomb peak and the associated Lomb periodogram.

In order to interpret the results presented in the figures 3 to 22, we need to explain the criteria that we have used. First, to make the description simpler and more geometrical, as shown in Fig. 3, we first classify all pairs of (H, q) into three classes: $\mathbf{W}$ (wedge or wall), $\mathbf{P}$ (platform) and $\mathbf{B}$ (bottom of valley or basin).

In Fig. 4, the pairs (H, q) near $(0.1, 0.1)$ gives the largest P_N, which implies the most significant log-periodic oscillations in the generalized q derivative. However, the associated ω is about $3 \sim 4$ as shown in the region $\mathbf{B}$ of Fig. 3. The problem is that this value is dangerously close to the most probable (log-periodic) angular-frequency $\omega^{mp} = 3.6$, resulting solely from the most probable noise. It was indeed shown [17] that noise decorating power laws may lead to artifactual log-periodicity with a most probable frequency corresponding roughly to 1.5 oscillations over the whole range of analysis. In the present context, this defines the most probable (log-periodic) angular frequency ω^{mp} by the following formula

$$\omega^{mp} = \frac{2\pi \times 1.5}{\ln(p_c - p_{\min}) - \ln(p_c - p_{\max})} \,, \tag{13}$$

where the acoustic emission signal is recorded from the pressure $p_{\min}$ to $p_{\max}$. In the case of experiment $\#\,1$, this leads to $\omega^{mp} = 3.6$. Thus, a value of ω in the range $3 \sim 4$ corresponds to approximately 1.5 oscillations in the plot of the generalized q-derivative as a function of $\ln(p_c - p)$ for the whole range of pressure. This is not sufficient. We should thus exclude these pairs of

(H, q). This defines our **second criterion** for qualifying the existence of log-periodicity: pairs of (H, q) with $\omega(H, q) \leq \omega^{mp}$ should be discarded, because there is a non-negligible probability that the observed log-periodicity may result from noisy fluctuations around the power law and is thus spurious. Ideally, we should estimate the probability that random noise, of several plausible standard distributions, creates a false alarm that a periodicity (or log-periodicity) is found in the (H, q)-derivative of the signal. This has been done in a systematic way for a large variety of noise, without and with long-range correlation [21]. However, it is difficult to identify what should be the correct null hypothesis of the noise decorating the generalized q-derivative. For the sake of simplicity, we thus stick to the simple rule called **second criterion** just discussed.

A log-periodic angular frequency which is too small may result from noise, as we just said. Similarly, a too high log-periodic angular frequency is also the signature of noise, simply because it is easy to fit noisy data with many oscillations. We should thus also discard the pairs of (H, q) whose ω are too large. Ref. [3] used this criterion to discard solutions with $\omega \geq 14$. This gives us a **third criterion**. It is not always obvious to fix the value of the threshold angular frequency beyond which solutions are rejected as noise. Fortunately, this third criterion can often be obtained to follow from the first criterion, since the Lomb peak P_N corresponding to a large angular frequency is usually low [21]. We apply this criterion and hence exclude (H, q) pairs in the regions of $\mathbf{W_1}$, $\mathbf{W_2}$ and $\mathbf{W_3}$ shown in Fig. 3.

A physically meaningful optimal pair of (H, q) is thus obtained. For data set $\#1$, it corresponds to $(H, q) = (-0.9, 0.5)$, which is indicated by arrows in Fig. 3 and Fig. 4. It lies within a platform shown in Fig. 3. We also show in Fig. 5 the generalized q-derivative and in Fig. 6 its corresponding Lomb periodogram. The log-periodic oscillations are found to be very significant. Under the null hypothesis of independent Gaussian noise decorating the signal, the false-alarm probability of the log-periodic component is $\approx 0.06\%$. The false-alarm probability for the null hypothesis of independent heavy-tailed noises (say, Lévy stable noise and power-law noise) and weakly correlated noises (say, Garch(1,1) noise and fractional Gaussian noise (fGn) with the Hurst index less than 0.5) is even lower [21]. If we assume a strongly correlated noise such as fractional Gaussian noise with the Hurst index greater than 0.5, the false-alarm probability increases: for instance, a fractional Gaussian noise with Hurst index of 0.62 leads to a false-alarm probability of 1% [21].

As a **fourth criterion**, if the majority of the pairs (H, q) have similar oscillatory behavior (i.e., similar ω), we take that this indicates a robust log-periodic signal and that the optimal pair should be within these pairs with high probability. This excludes $\mathbf{W_1}$, $\mathbf{W_2}$, $\mathbf{W_3}$ and $\mathbf{W_4}$ in Fig. 3 and strengthens the choice of the previous criteria. This fourth criterion is sometimes ambiguous to apply in practice. However, all experimental systems have their optimal pair (H, q) in well-defined platforms $\mathbf{P}$, except for experiment $\#3$ which presents its optimal (H, q) in $\mathbf{W_1}$.

Table 1 summurizes the results of the (H, q)-analysis on the energy release rate of data sets $\#1$, $\#2$, $\#3$, $\#4$ and $\#6$. For each data set, the generalized q-analysis was performed between $(p_{\min}, p_{\max})$, with a number of points varying between 55 and 164 as indicated in the column "Points." p_c is the true critical pressure at rupture. P_N is the optimal value of the Lomb peak height, and ω is the corresponding logarithmic angular frequency. The column "Gaussian" presents the false-alarm probability of the Lomb peak under the null hypothesis of independent Gaussian noise. The column "fGn" evaluates the value of the Hurst index of a fractional Brownian noise which would give a false-alarm probability 1% to get the same peak as in our analysis.

These results give a very strong confidence that there is a genuine log-periodicity of the energy release rate before rupture in the data sets $\#1$, $\#2$, $\#3$, $\#4$ and $\#6$. This confirms and strengthens Ref. [3], which claimed that a pure power law fails to parameterize the data but a log-periodic formulae does a good job.

Tank	Points	$p_{\min}$	$p_{\max}$	p_c	(H,q)	P_N	ω	ω'	ω^{mp}	N_{osc}	Gaussian	fGn
$\#1$	131	453.5	694.5	713	$(-0.9, 0.5)$	9.7	5.7	23.3	3.6	2.4	8E-3	0.56
$\#2$	147	451.5	660.5	673	$(0.1, 0.1)$	33.8	8.6	/	3.3	3.9	3E-13	0.92
$\#3$	121	538.5	756.5	764	$(-0.2, 0.1)$	23.1	12.4	6.8	2.8	6.6	1E-8	0. 82
$\#4$	55	671.5	744.5	756	$(0, 0.4)$	8.7	4.7	17.0	4.7	1.5	9E-3	0.52
$\#6$	164	451.5	723.5	734	$(0.1, 0.2)$	15.8	6.2	/	2.9	3.2	2E-5	0.71

Table 1: Summary of the results of the (H,q)-analysis on the energy release rate of data sets $\#1$, $\#2$, $\#3$, $\#4$ and $\#6$. For each data set, the generalized q-analysis was performed between $(p_{\min}, p_{\max})$ with a number of points given in the column "Points." p_c is the true critical pressure of rupture. The column (H,q) lists the optimal pairs. P_N is the optimal value of the Lomb peak height. ω and ω' are the corresponding logarithmic angular frequency and the angular frequency corresponding to the second highest peak. N_{osc} is the number of oscillations. The column "Gaussian" presents the false-alarm probability of the Lomb peak under null hypothesis of independent Gaussian noise. The column "fGn" gives the Hurst index of a fractional Gaussian noise that would give a false-alarm probability 1% to obtain the same Lomb peak as in the signal.

3.2 Cumulative energy release

We follow the same procedure as in the previous section to analyze the cumulative energy release of the same five experimental data sets discussed previously. We use slightly different truncations in this analysis of the cumulative energy release. The results obtained for the five data sets are shown in Figs. 23 to 42. Figures 24, 28, 32, 36 and 40 show the dependence of the highest peak $P_N(H,q)$ in each Lomb periodogram as a function of H and q. Figs. 23, 27, 31, 35 and 39 are plots of the associated logarithmic angular frequencies $\omega(H,q)$. The generalized q-derivative of the cumulative energy release corresponding to the optimal pairs of (H,q) for the five data sets are illustrated respectively in Figs. 25, 29, 33, 37 and 41 with their Lomb periodograms shown in Figs. 26, 30, 34, 38 and 26.

In Fig. 24, the largest P_N's are in the region $\mathbf{B}$. However, the corresponding frequencies are very low as shown in Fig. 23 which gives the most probable frequency. Hence we excludes region $\mathbf{B}$ in accordance with the second criterion. The optimal pair in the platform $\mathbf{P}$ is $(H=-0.5, q=0.6)$. One can observe a platform of ω in Fig. 23, which is consistent with the fourth criterion. In Fig. 25, the log-periodic oscillations of the (H,q)-derivative are clearly visible, and correspond to the high Lomb peak shown in Fig. 26. The log-periodic oscillations become even strongly and more significant if more points are discarded at the low and high pressure ends of the data set.

Data set $\#2$ is more noisy and a major part of the pairs (H,q) give very low frequencies close to ω^{mp}, as shown in Fig. 27, which lead us to exclude all the local maxima shown in Fig. 28. The optimal pair $(0.3, 0.1)$ is located at the wedge $(\mathbf{W_3})$ indicated by an arrow (in contradiction the fourth criterion). The log-periodicity is quite apparent in Fig. 29. Correspondingly, its Lomb peak shown in Fig. 30 is very significant. The data sets $\#3$ and $\#4$ are similar to $\#2$. For $\#6$, the optimal pair $(-0.3, 0.8)$ located on the platform shown in Fig. 39 has a local maximum shown in Fig. 40. We summarize all these results in Table 2.

3.3 Comparison between energy release rates and their cumulative

Comparing Table 1 and Table 2, we find that the cumulative energy releases present a more significant log-periodic component. Taking the cumulative corresponds to perform a low-pass filter that smooths out significantly the noise and usually provides better signals with higher signal-to-noise

Tank	Points	$p_{\min}$	$p_{\max}$	p_c	(H,q)	P_N	ω	ω'	ω^{mp}	N_{osc}	Gaussian	fGn
$\#1$	144	453.5	711.5	713	$(-0.5, 0.6)$	51.7	5.5	/	1.8	4.6	5E-21	0. 98
$\#2$	138	467.5	661.5	673	$(0.3, 0.2)$	34.4	10.0	5.3	3.3	4.5	2E-13	0. 93
$\#3$	63	671.5	756.5	764	$(-0.2, 0.4)$	14.5	4.5	9.9	3.8	1.8	5E-5	0.70
$\#4$	56	671.5	746.5	756	$(0, 0.6)$	19.0	5.5	17.5	4.3	1.9	3E-7	0.79
$\#6$	72	614.5	723.5	734	$(-0.3, 0.8)$	15.7	12.7	5.4	3.9	4.9	1E-5	0.71

Table 2: Summary of the results of the (H,q)-analysis on the cumulative energy release of data sets $\#1$, $\#2$, $\#3$, $\#4$ and $\#6$. The meaning of the columns are the same as in Table 1.

ratio. Of course, taking the cumulative also reduces the amplitude of the underlying log-periodic oscillations. There is thus a compromise. As an illustration, let us compare Fig. 13 and Fig. 33. It is clear that the (H,q)-derivative of the energy release rate in Fig. 13 is much more noisy than that of the cumulative energy release shown in Fig. 33. On the other hand, the high-frequency oscillations which are clearly visible in Fig. 33 are suppressed in Fig. 33 and can not be captured by the Lomb analysis. Thus, the log-frequency with largest peak power of the energy rate ($f = 1.97$) is much higher than that of the cumulative energy ($f = 0.72$). We note however that the second highest peak in Fig. 33 corresponds to the highest peak of the energy release rate.

In general, we find that the cumulative energy release keeps the same underlying log-periodic structure as found in the energy release rate. We observe that data sets $\#1$, $\#2$ and $\#4$ have very similar logarithmic frequencies for the energy release rate and their cumulative. Most Lomb periodograms exhibit harmonics of each other. This close correspondence obtained in the (H,q)-analysis provides a better characterization of the log-periodic nature in the system than obtained previously with the parameterization approach of fitting the data sets with a log-periodic function [3].

Finally, we note that all data sets exhibit a fundamental value of the logarithmic angular frequency which is compatible with the value $\omega = 5.8 \pm 0.9$. In some cases, it is its second harmonic that gives the strongest peak of the Lomb periodograms. This value corresponds to a preferred scaling ratio $\lambda = e^{2\pi/\omega} = 3.0 \pm 0.5$.

4 Post-diction of ruptures

The (H,q)-analysis has shown its power for detecting log-periodicity, conditioned on our knowledge of the critical pressure p_c at rupture. It is natural to ask whether it can be extended to provide advanced prediction of p_c. For carrying these tests, we use the cumulative energy release which provided the strongest log-periodic signal in the analysis reported in previous sections. Our strategy is to use each data up to a maximum pressure $p_{\max} < p_c$, assume some value for p_c and perform the same analysis as in section 3. i.e., for a given presumed critical points p_c, we determine the optimal pair (H,q). For each presumed p_c, we thus obtain the Lomb peak height $P_N(H,q)$ and its associated logarithmic angular frequency $\omega(H,q)$ as a function of H and q. In order to find the optimal (H,q) corresponding to the maximum $P_N(H,q)$, we add the second criterion to exclude those (H,q) with $\omega(H,q) \leq \omega^{mp}$. Having determined the optimal $P_N(p_c)$ and $\omega(p_c)$ as functions of the presumed critical pressure p_c, we determine the predicted critical pressure $\hat{p}_c$ by the condition

$$P_N(\hat{p}_c) = \max_{p_c}\{P_N(p_c)\}, \tag{14}$$

without further constraints on $\omega(p_c)$.

Tank	Points	$p_{\min}$	$p_{\max}$	ω	p_c	$\frac{p_c - p_{\max}}{p_c}$	$\hat{p}_c^{(1)}$	$\hat{p}_c^{(2)}$
$\#1$	139	453.5	705.5	5.5	713	1.1%	722.5(734)	722.5(761)
$\#2$	149	452.5	662.5	5	673	1.6%	680.5(681)	686.5(700)
$\#3$	65	671.5	759.5	4.5	764	0.6%	763.5(765)	767.5(772)
$\#4$	56	671.5	746.5	5.5	756	1.3%	755.5(755)	755.5(763)
$\#6$	74	614.5	726.5	6.4	734	1.0%	742.5(744)	758.5(759)

Table 3: Post-diction using the (H, q)-analysis on the cumulative energy release of tanks $\#1$, $\#2$, $\#3$, $\#4$ and $\#6$. Columns $\hat{p}_c^{(1)}$ and $\hat{p}_c^{(2)}$ list the predicted critical pressure $\hat{p}_c$ and its corresponding upper threshold in the parenthesis with the constraint (16) for $k = 4/3$ and $k = 1$ respectively. The meaning of the other columns are the same as in Table 1.

In practice, we analyze the function $P_N(p_c; H, q)$ of the three variables p_c, H and q in the following sequence: we fix a value for p_c and explore the plane (H, q). We then change p_c and redo the exploration of the plane (H, q), etc. Fig. 43 through 47 give the optimal Lomb peak height P_N as a function of the presumed critical pressure p_c. It is obvious that this scheme does not give a good predictive skill, as the most important pattern observed in these figures is the systematic increasing trend, tending to reject the predicted p_c towards too large values.

We thus attempt to improve this prediction skill by requesting that the predicted p_c should not be too far from the last point, i.e., it is nonsensical to hope to predict too far from the "present." To implement this idea, we impose $\omega > k\omega^{mp}$, namely,

$$\frac{\omega}{2\pi} > \frac{1.5k}{\ln(p_c - p_{\min}) - \ln(p_c - p_{\max})}, \tag{15}$$

where $k \geq 1$ is a "safety factor." This constraint translates into the following condition for p_c:

$$p_c < p_{\max} + \frac{p_{\max} - p_{\min}}{e^{\frac{3k\pi}{\omega}} - 1}. \tag{16}$$

This constraint (16) means that there exists an upper threshold beyond which we can not make a physically meaningful prediction. Since the left-hand-side of (16) is monotonously increasing with ω, it is possible to make a prediction much earlier before the critical point, the larger ω is. This is natural since large ω implies more log-periodic oscillations and thus a stronger log-periodic signal. To implement this condition in practice, we take $\omega = 5.8$ as the central value of the log-periodic angular frequency. According to this constraint (16), ruptures of tanks $\#5$ and $\#7$ are unpredictable, since the last point $p_{\texttt{last}}$ is too far from the true critical pressure.

The results are given in Table 3. The columns $\hat{p}_c^{(1)}$ and $\hat{p}_c^{(2)}$ list the predicted critical pressure $\hat{p}_c$ and its corresponding upper threshold in the parenthesis with the constraint (16) for the two choices $k = 4/3$ and $k = 1$ respectively. The prediction for experiment $\#1$ is very good. For the other experiments, $\hat{p}_c$ is found to be very close to the upper threshold. The predictions for experiments $\#2$, $\#3$ and $\#4$ are reasonable while the prediction for case $\#6$ fails completely.

Acknowledgments: We are grateful to A. Erzan for a discussion on Jackson's integral and for supplying the corresponding references. This work was supported by NSF-DMR99-71475 and the James S. Mc Donnell Foundation 21st century scientist award/studying complex system.

APPENDIX A

From the definition (8), the extremal condition $dg(x)/dx = 0$ gives the extreme points of $g(x)$ solutions of

$$C_1 \sin(\omega \ln x) - C_2 \cos(\omega \ln x) = 0 \,, \tag{17}$$

that is,

$$\omega \ln(x_m) = n\pi + \arctan(C_2/C_1), \tag{18}$$

where $n = 0, \pm 1, \pm 2, \cdots$. It follows that the extreme values of $g(x)$ are

$$g(x_m) = \pm\sqrt{C_1^2 + C_2^2} \,. \tag{19}$$

When $\omega \ln(x_m) = 2n\pi + \arctan(C_2/C_1)$, $g(x_m) = \sqrt{C_1^2 + C_2^2}$ is the maximum; when $\omega \ln(x_m) = (2n+1)\pi + \arctan(C_2/C_1)$, $g(x_m) = -\sqrt{C_1^2 + C_2^2}$ is the minimum. This is proved by the following exhaustive classification.

1. $e^{(2k-1)\pi/\omega} < q < e^{2k\pi/\omega}$, with $k = 0, \pm 1, \pm 2, \cdots$.

   In this case, $C_2 < 0$. Thus $-\pi/2 < \arctan(C_2/C_1) < 0$. When $\omega \ln(x_m) = 2n\pi + \arctan(C_2/C_1)$, $\cos(\omega \ln x_m) > 0$ and $\sin(\omega \ln x_m) < 0$, and thus $g(x_m) = \sqrt{C_1^2 + C_2^2}$ is the maximum. When $\omega \ln(x_m) = (2n+1)\pi + \arctan(C_2/C_1)$, $\cos(\omega \ln x_m) < 0$ and $\sin(\omega \ln x_m) > 0$, and thus $g(x_m) = -\sqrt{C_1^2 + C_2^2}$ is the minimum.

2. $q = e^{k\pi/\omega}$, with $k = 0, \pm 1, \pm 2, \cdots$.

   In this case, $C_2 = 0$. Thus $\arctan(C_2/C_1) = 0$ and $g(x) = C_1 \cos(\omega \ln x)$. When $\omega \ln(x_m) = 2n\pi$, $g(x_m) = C_1$ is the maximum. When $\omega \ln(x_m) = (2n+1)\pi$, $g(x_m) = -C_1$ is the minimum.

3. $e^{2k\pi/\omega} < q < e^{(2k+1)\pi/\omega}$, with $k = 0, \pm 1, \pm 2, \cdots$.

   In this case, $C_2 > 0$. Thus $0 < \arctan(C_2/C_1) < \pi/2$. When $\omega \ln(x_m) = 2n\pi + \arctan(C_2/C_1)$, $\cos(\omega \ln x_m) > 0$ and $\sin(\omega \ln x_m) > 0$, and thus $g(x_m) = \sqrt{C_1^2 + C_2^2}$ is the maximum. When $\omega \ln(x_m) = (2n+1)\pi + \arctan(C_2/C_1)$, $\cos(\omega \ln x_m) < 0$ and $\sin(\omega \ln x_m) < 0$, and thus $g(x_m) = -\sqrt{C_1^2 + C_2^2}$ is the minimum.

The amplitude of $D_q^H y(x)$ is then

$$A = C'\sqrt{C_1^2 + C_2^2}\,(x_m)^{m-H}, \tag{20}$$

while the local extreme values are

$$D_m = \left(B' \pm C'\sqrt{C_1^2 + C_2^2}\right)(x_m)^{m-H}. \tag{21}$$

References

[1] J.-C. Anifrani, C. Le Floc'h, D. Sornette and B. Souillard, J.Phys.I France 5, 631 (1995).

[2] J.-C. Anifrani, C. Le Floc'h and D. Sornette, Contrôle Industriel **220**, 43 (1999).

[3] A. Johansen and D. Sornette, Eur. Phys. J. B 18, 163-181 (2000).

[4] D. Sornette and C. Vanneste, Phys. Rev. Lett. 68, 612 (1992); C. Vanneste and D. Sornette, J.Phys.I France 2, 1621 (1992); D. Sornette , C. Vanneste and L. Knopoff, Phys.Rev.A 45, 8351 (1992).

[5] A. Garcimartin, A. Guarino, L. Bellon, and S. Ciliberto, Phys. Rev. Lett. 79, 3202 (1997); A. Guarino, A. Garcimartin, and S. Ciliberto, Eur. Phys. J. B 6, 13 (1998); A. Guarino, S. Ciliberto, and A. Garcimartin, Europhysics Letters 47, 456 (1999).

[6] J.V. Andersen, D. Sornette and K.-T. Leung, Phys. Rev. Lett. 78, 2140-2143 (1997); D. Sornette, K.-T. Leung and J.V. Andersen, Phys. Rev. Lett. 80, 3158 (1998).

[7] A. Johansen and D. Sornette, Int. J. Mod. Phys. C 9, 433 (1998).

[8] M. Sahimi and S. Arbabi, Phys. Rev. Lett. 77, 3689 (1996).

[9] Y. Huang, G. Ouillon, H. Saleur and D. Sornette, Phys. Rev. E 55, 6433 (1997).

[10] D. Sornette, Physics Reports 297, 239 (1998).

[11] H. Saleur and D. Sornette, J. Phys. I France 6, 327-355 (1996).

[12] F.H. Jackson, Q. J. Pure. Appl. Math 41, 193 (1910); Q. J. Math Oxford Ser. 2, 1 (1951).

[13] A. Erzan, Phys. Letts. A 225, 235 (1997).

[14] A. Erzan and J.-P. Eckmann, Phys. Rev. Letts. 78, 3245 (1997).

[15] D. Sornette and C.G. Sammis, J.Phys.I France 5, 607-619 (1995); H. Saleur, C.G. Sammis and D. Sornette, J. Geophys. Res. 101, 17661-17677 (1996); A. Johansen, D. Sornette, H. Wakita, U. Tsunogai, W.I. Newman and H. Saleur, J.Phys.I France 6, 1391-1402 (1996); A. Johansen, H. Saleur and D. Sornette, Eur. Phys. J. B 15, 551-555 (2000); Y. Huang, H. Saleur and D. Sornette, J. Geophys. Research 105, 28111-28123 (2000)

[16] G. Ouillon and D. Sornette, Geophys. J. Int. 143, 454-468 (2000).

[17] Y. Huang, A. Johansen, M. W. Lee, H. Saleur and D. Sornette, J. Geophys. Res. 105, 25451-25471 (2000).

[18] M.W. Lee and D. Sornette, Eur. Phys. J. B 15, 193-197 (2000).

[19] D. Sornette, A. Johansen and J.-P. Bouchaud, J.Phys.I France 6, 167-175 (1996); D. Sornette and A. Johansen, Physica A 245, 411-422 (1997); A. Johansen and D. Sornette, RISK 12 (1), 91-94 (1999); Eur. Phys. J. B 9, 167-174 (1999); Johansen, A., D. Sornette and O. Ledoit, J. Risk 1, 5-32 (1999); A. Johansen, O. Ledoit and D. Sornette, Int. J. Theor. Appl. Fin. 3 (2), 219-255 (2000); Johansen, A. and D. Sornette, Eur. Phys. J. B 17, 319-328 (2000); A. Johansen and D. Sornette, Int. J. Theor. Appl. Fin. 4 (6), 853-920 (2001); D. Sornette and A. Johansen, Quantitative Finance 1 (4), 452-471 (2001).

[20] Press, W.H., Teulolsky, S.A., Vetterlong, W.T. and Flannery, B.P., Numerical Recipies in Fortran, Cambridge University Press (1994).

[21] Zhou, W.-X. and D. Sornette, Statistical significance of periodicity and log-periodicity with heavy-tailed correlated noise, Int. J. Mod. Phys. C 13 (2) February (2002) (e-print at http://arXiv.org/abs/cond-mat/0110445)

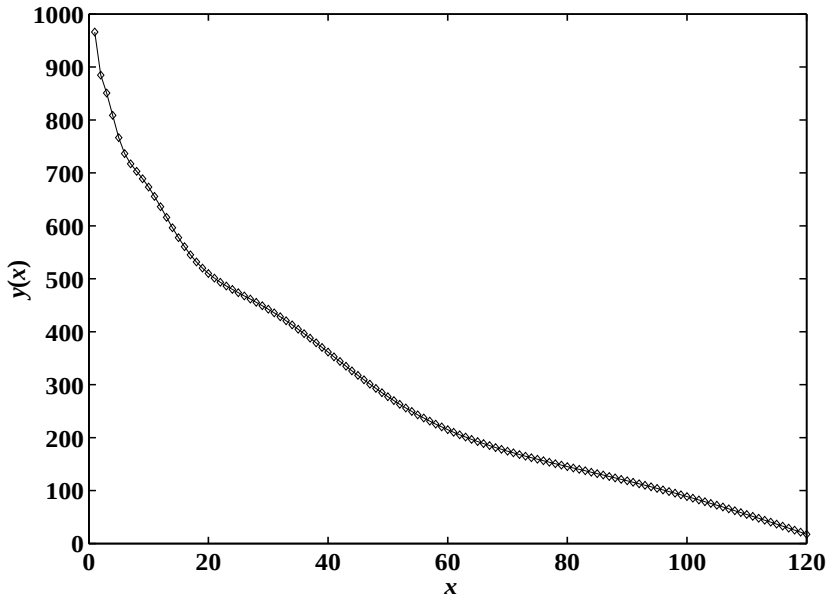

Figure 1: Plot of $y(x)$ defined by Eq. (5) as a function of the pressure-to-rupture x with $A = 1260$, $B = 300$, $C = 6$, $m = 0.3$, $\omega = 5.4$ and $\phi = 0$. We generated 120 evenly spaced data points with x between 1 and 120, to mimic the cumulative energy release of a real acoustic emission experiment.

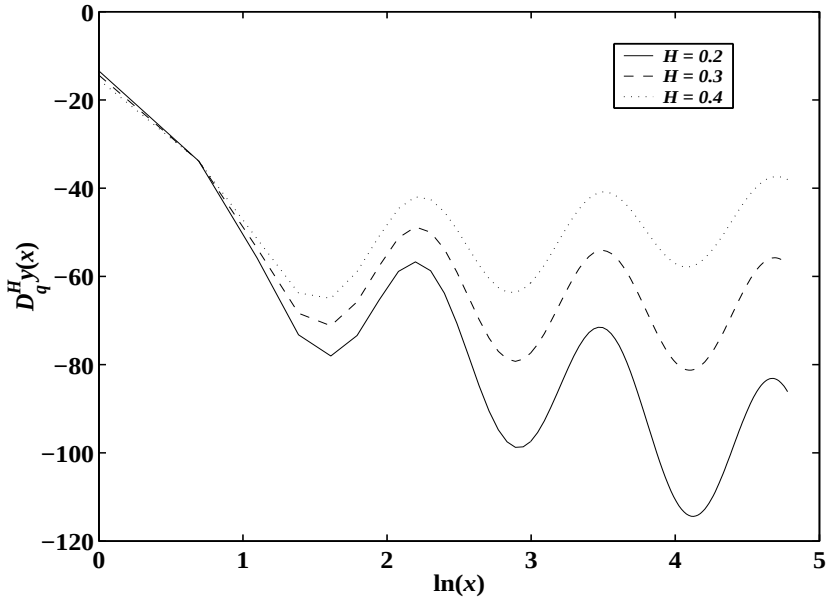

Figure 2: The generalized q-derivative of $y(x)$ shown in Fig. 1 with $q = 0.5$ for $H = 0.2$, $H = 0.3$ and $H = 0.4$, respectively. The calculation assumes a critical point at $x_c = 1$ while the synthetic function has its genuine critical point at $x_c = 0$. This incorrect value of the critical point in the calculation of the generalized q-derivative is responsible for the distortions observed for $x < 1$.

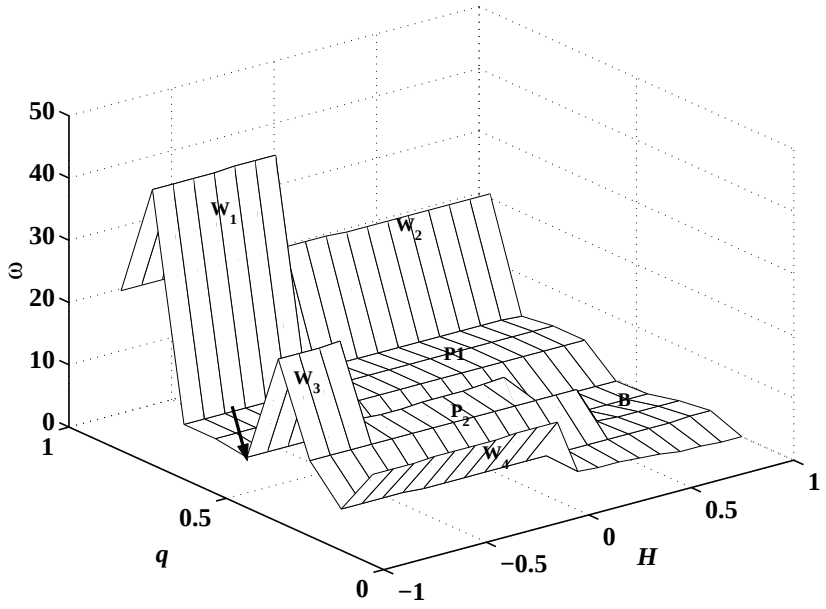

Figure 3: Dependence of the logarithmic angular frequency $\omega(H, q)$ of the most significant peak in each Lomb periodogram of the (H, q)-derivative of the energy release rate before the rupture of tank $\#1$. The regions $\mathbf{W_1}$, $\mathbf{W_2}$, $\mathbf{W_3}$, $\mathbf{W_4}$ and $\mathbf{B}$ are excluded and the optimal pair $(-0.9, 0.5)$ is indicated by an arrow in the platform $\mathbf{P_1}$.

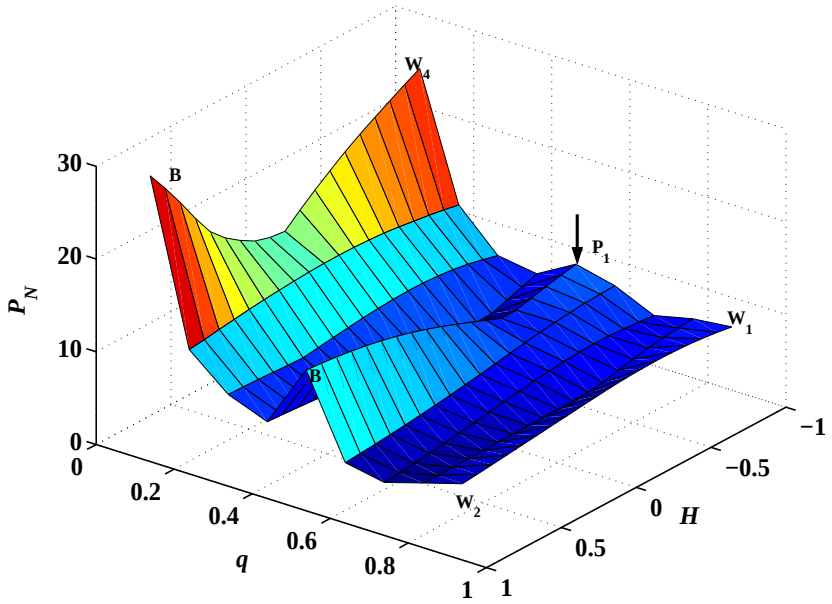

Figure 4: Dependence of the height $P_N(H, q)$ of the most significant peak in each Lomb periodogram of the (H, q)-derivative of the energy release rate before the rupture of tank $\#1$. The optimal pair $(-0.9, 0.5)$ is indicated by an arrow in the platform $\mathbf{P_1}$.

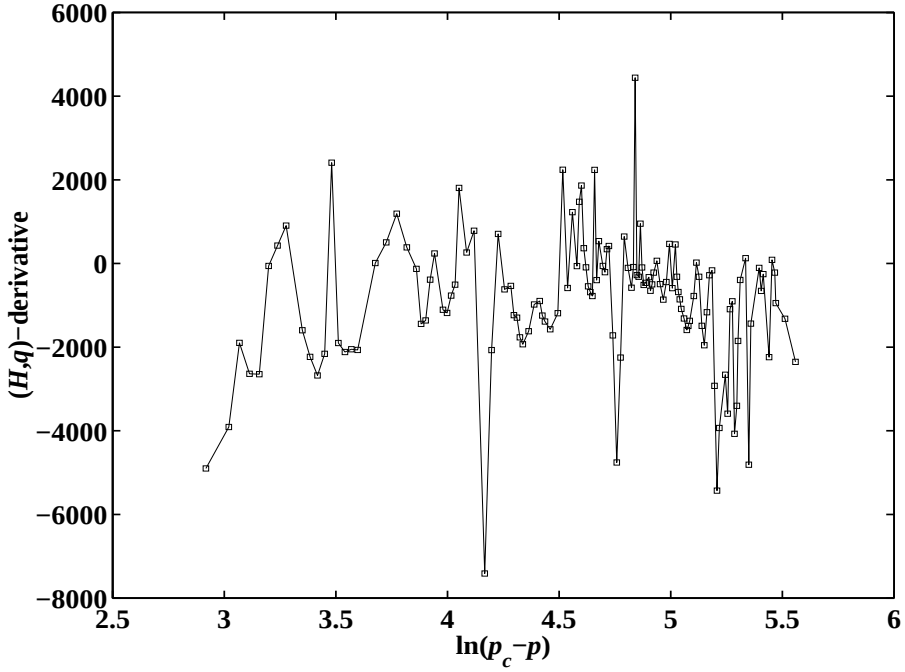

Figure 5: (H, q)-derivative of the energy release rate before the rupture of tank $\#\,1$ as a function of the pressure-to-rupture $p_c - p$ with $q = 0.5$ and $H = -0.9$.

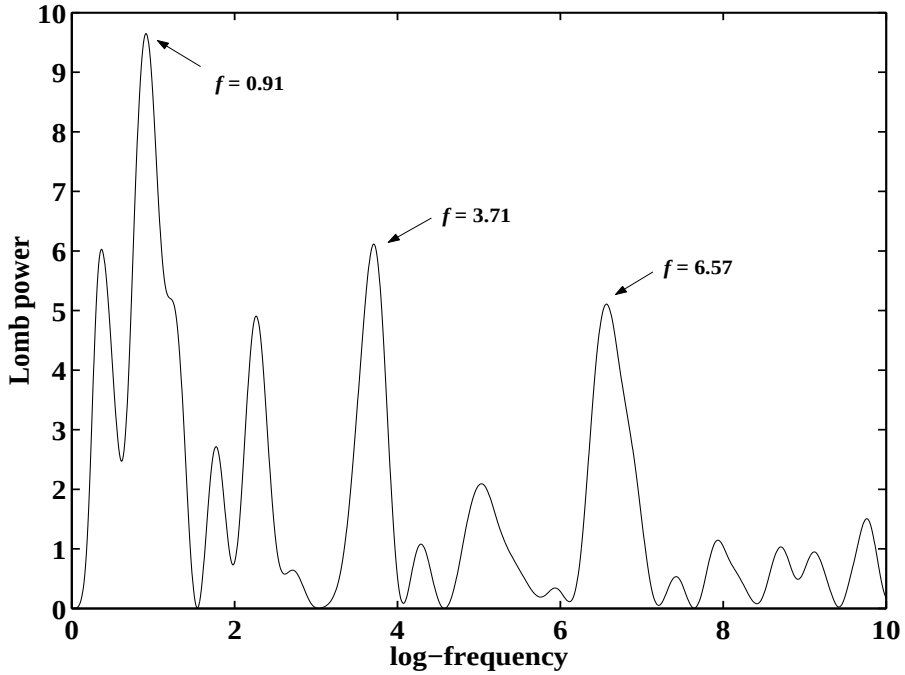

Figure 6: Lomb power of the (H, q)-derivative shown in Fig. 5. The log-frequency is 0.91 which has two clear harmonics at 3.71 and 6.57.

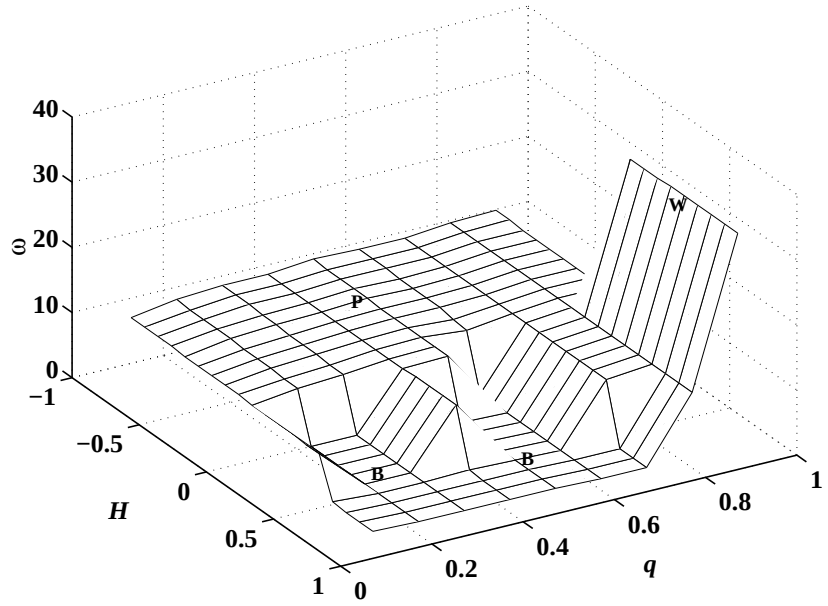

Figure 7: Dependence of the logarithmic angular frequency $\omega(H, q)$ of the most significant peak in each Lomb periodogram of the (H, q)-derivative of the energy release rate before the rupture of tank $\#\,2$. The wall **W** is excluded by both the third and the fourth criteria, while **B** is excluded by the second criterion.

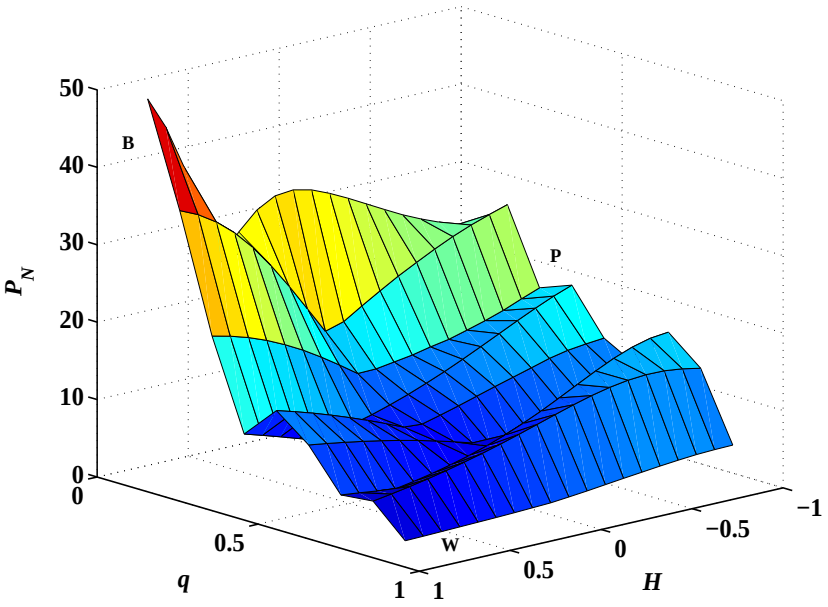

Figure 8: Dependence of the height $P_N(H, q)$ of the most significant peak in each Lomb periodogram of the (H, q)-derivative of the energy release rate before the rupture of tank $\#\,2$.

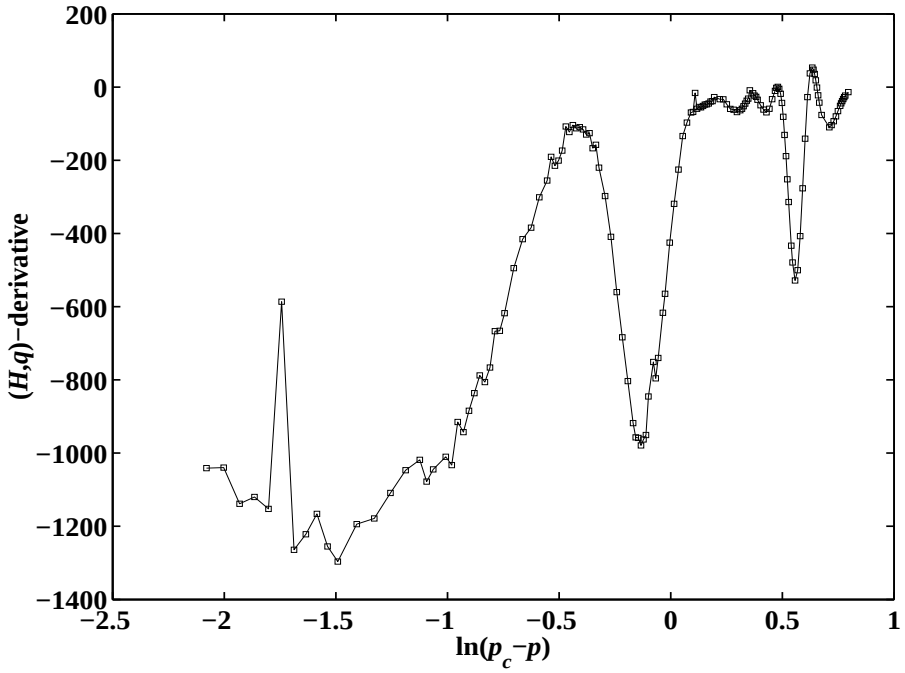

Figure 9: (H, q)-derivative of the energy release rate before the rupture of tank $\#\,2$ as a function of the pressure-to-rupture $p_c - p$ with $q = 0.1$ and $H = 0.1$.

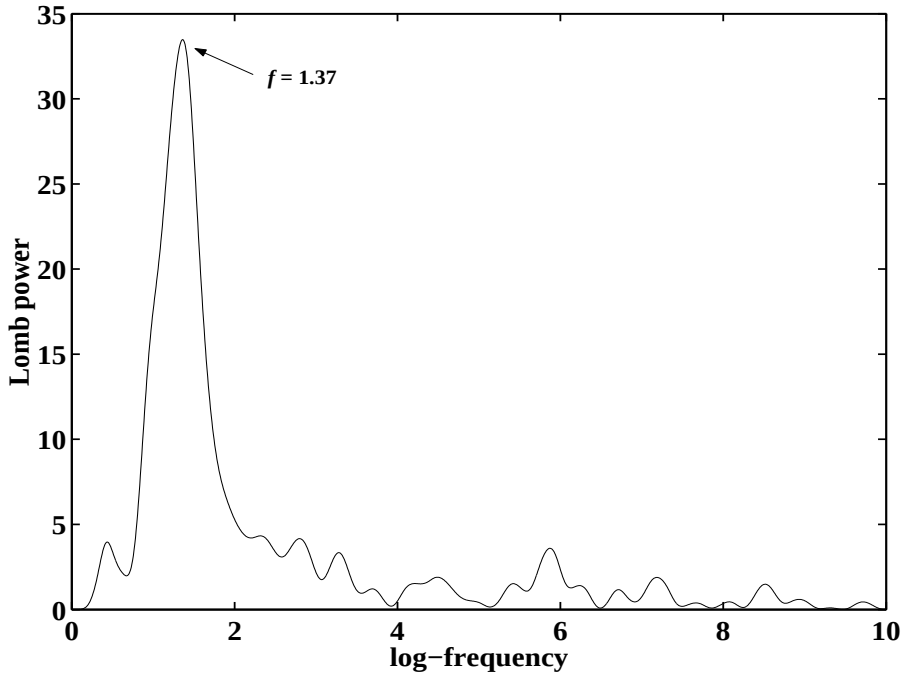

Figure 10: Lomb power of the (H, q)-derivative shown in Fig. 9.

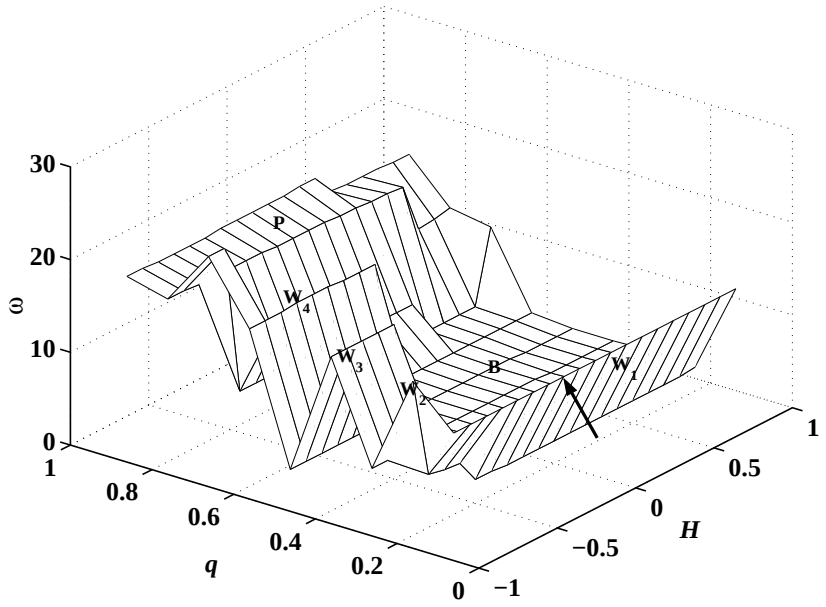

Figure 11: Dependence of the logarithmic angular frequency $\omega(H, q)$ of the most significant peak in each Lomb periodogram of the (H, q)-derivative of the energy release rate before the rupture of tank $\#3$. Regions $\mathbf{B}$ and $\mathbf{W_2}$, $\mathbf{W_3}$, $\mathbf{W_4}$ and $\mathbf{P}$ are excluded by the second and the third criteria, respectively. The fourth criterion is not used in this case and the optimal pair $(-0.2, 0.1)$ is at a wall $\mathbf{W_1}$ as indicated by an arrow.

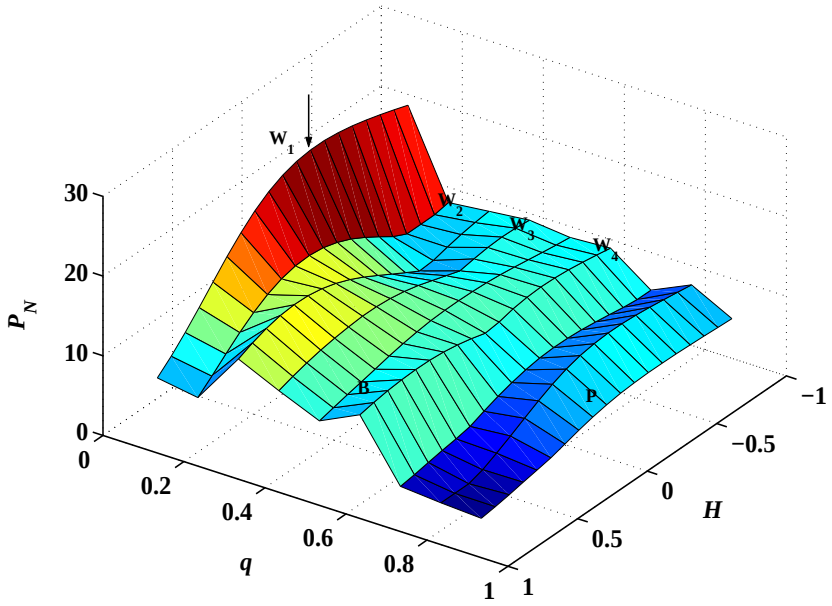

Figure 12: Dependence of the height $P_N(H, q)$ of the most significant peak in each Lomb periodogram of the (H, q)-derivative of the energy release rate before the rupture of tank $\#3$.

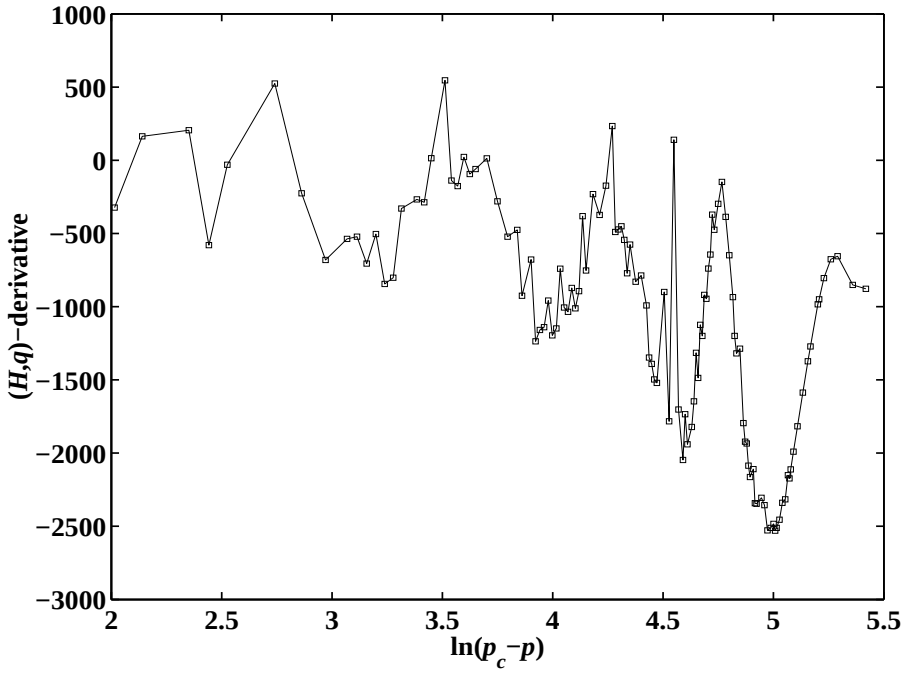

Figure 13: (H, q)-derivative of the energy release rate before the rupture of tank $\#\,3$ as a function of the pressure-to-rupture $p_c - p$ with $q = 0.1$ and $H = -0.2$.

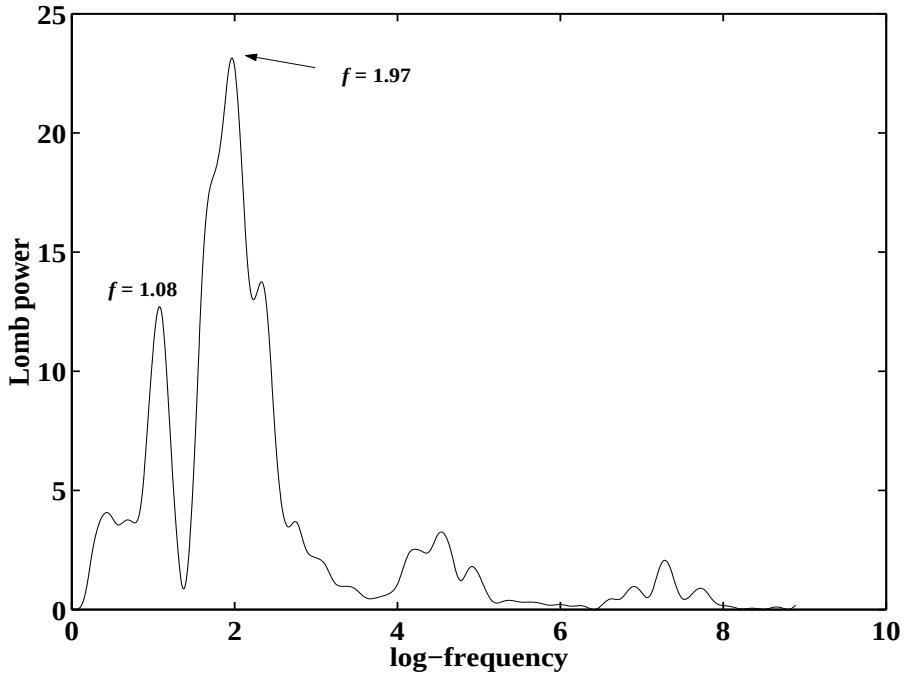

Figure 14: Lomb power of the (H, q)-derivative shown in Fig. 13.

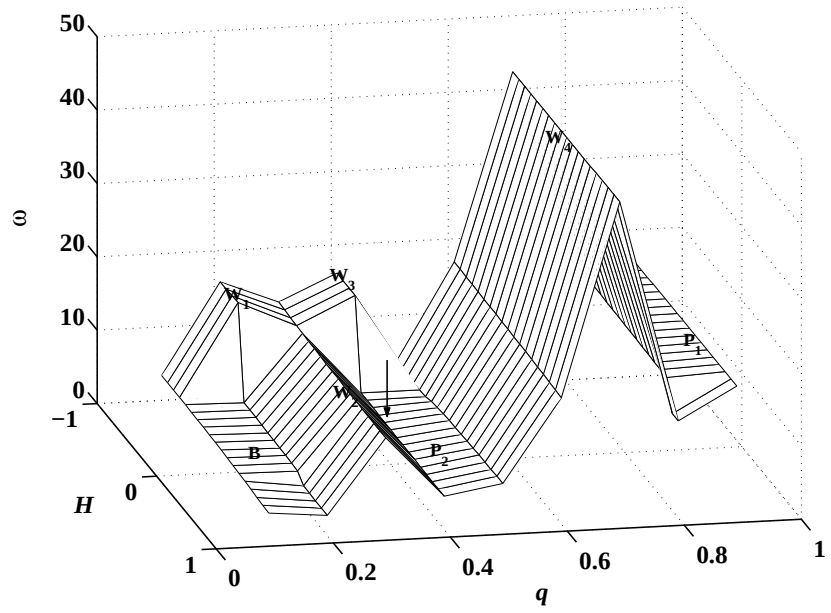

Figure 15: Dependence of the logarithmic angular frequency $\omega(H, q)$ of the most significant peak in each Lomb periodogram of the (H, q)-derivative of the energy release rate before the rupture of tank $\#\,4$. The optimal pair $(0.3, 0.4)$ is in the platform $\mathbf{P_2}$ indicated by an arrow.

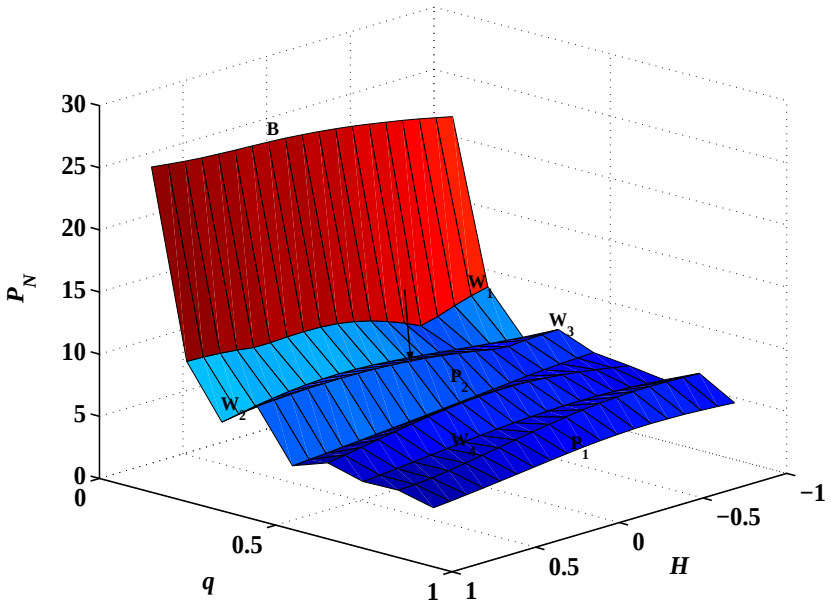

Figure 16: Dependence of the height $P_N(H, q)$ of the most significant peak in each Lomb periodogram of the (H, q)-derivative of the energy release rate before the rupture of tank $\#\,4$.

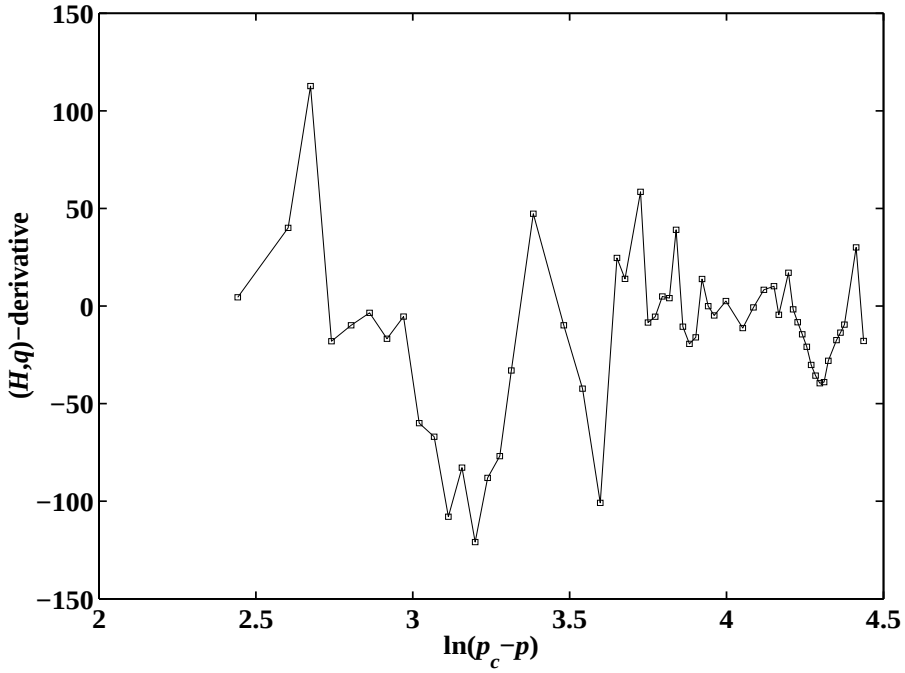

Figure 17: (H, q)-derivative of the energy release rate before the rupture of tank $\#\,4$ as a function of the pressure-to-rupture $p_c - p$ with $q = 0.4$ and $H = 0.3$.

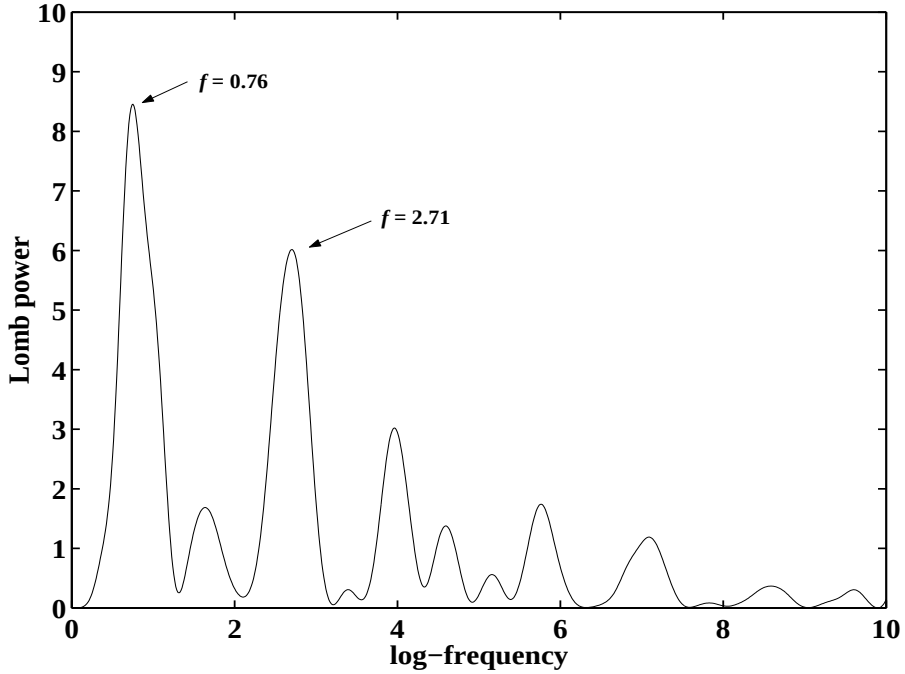

Figure 18: Lomb power of the (H, q)-derivative shown in Fig. 17. The fundamental log-frequency $f = 0.76$ and its harmonic $f = 2.71$ are indicated by arrows.

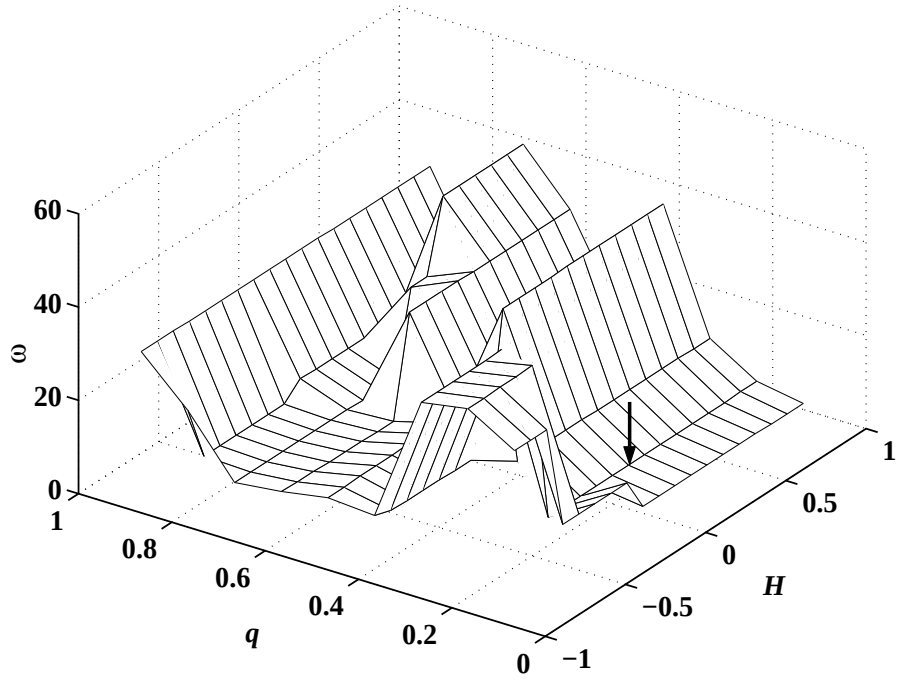

Figure 19: Dependence of the logarithmic angular frequency $\omega(H, q)$ of the most significant peak in each Lomb periodogram of the (H, q)-derivative of the energy release rate before the rupture of tank $\#\,6$. The optimal pair $(0.1, 0.2)$ is indicated by an arrow.

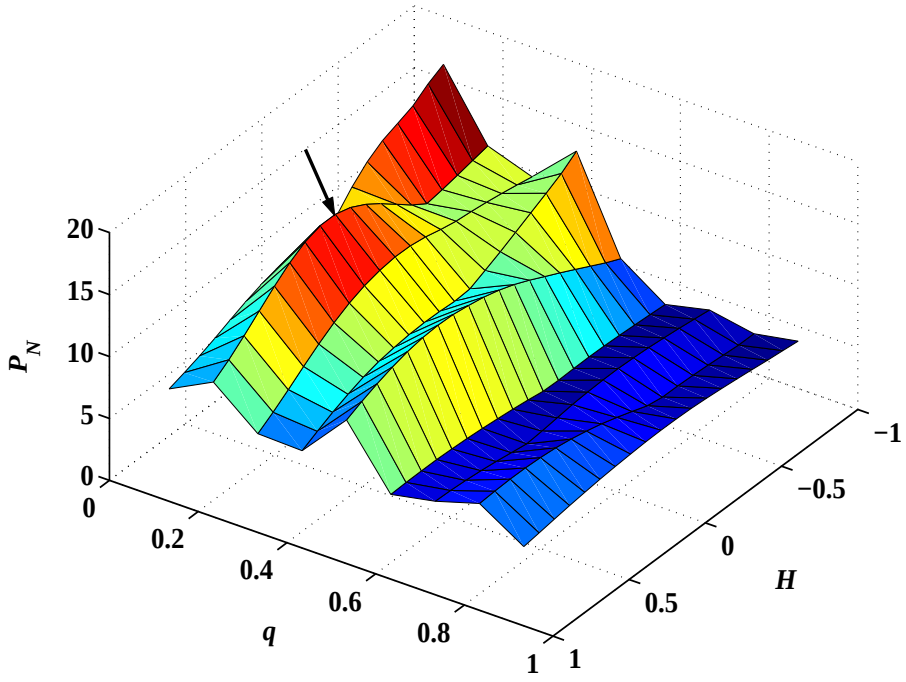

Figure 20: Dependence of the height $P_N(H, q)$ of the most significant peak in each Lomb periodogram of the (H, q)-derivative of the energy release rate before the rupture of tank $\#\,6$.

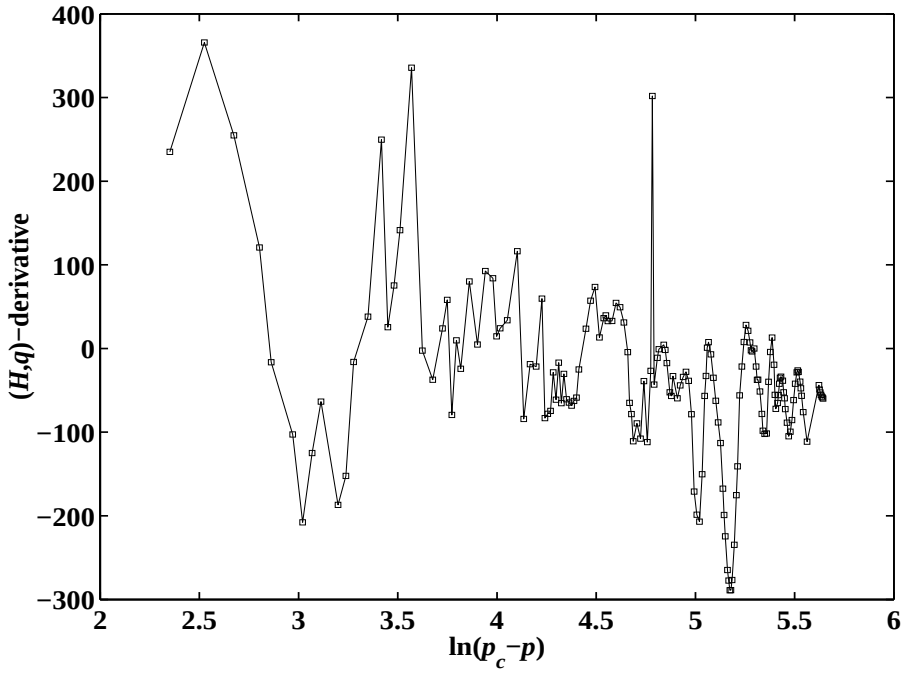

Figure 21: (H, q)-derivative of the energy release rate before the rupture of tank $\#\,6$ with respect to the pressure-to-rupture $p_c - p$ with $q = 0.2$ and $H = 0.1$.

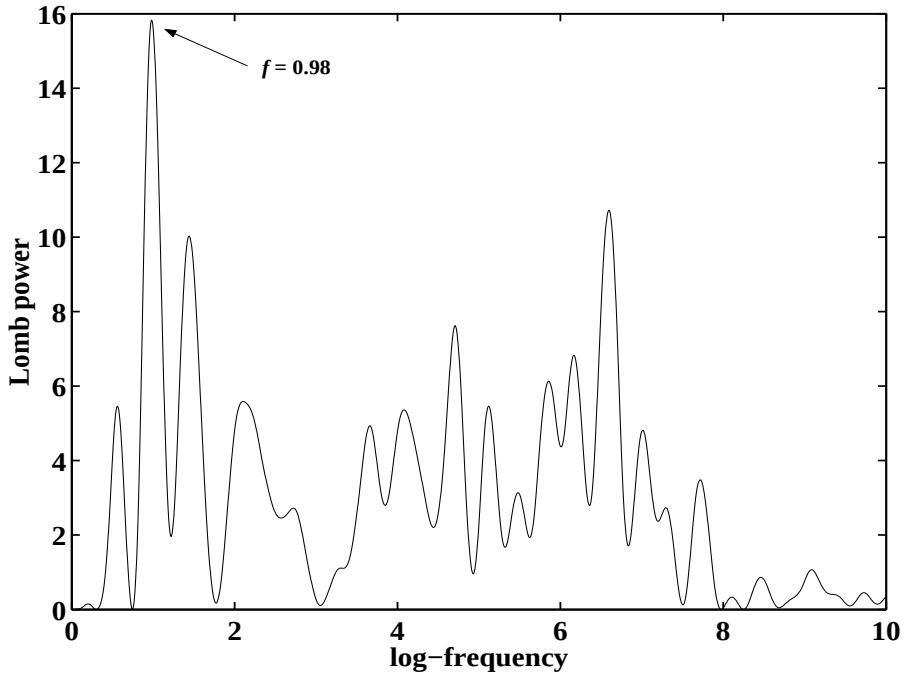

Figure 22: Lomb power of the (H, q)-derivative shown in Fig. 21.

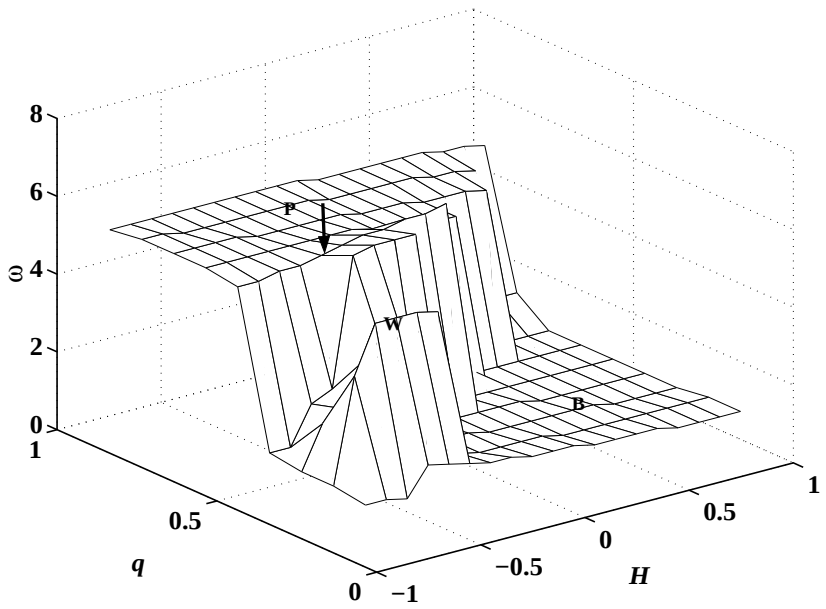

Figure 23: Dependence of the logarithmic angular frequency $\omega(H, q)$ of the most significant peak in each Lomb periodogram of the (H, q)-derivative of the cumulative energy release before the rupture of tank $\#\,1$. The wedge $\mathbf{W}$ and the bottom $\mathbf{B}$ are excluded by the second and fourth criteria. The optimal pair $(-0.5, 0.6)$ is indicated by an arrow in the platform $\mathbf{P}$.

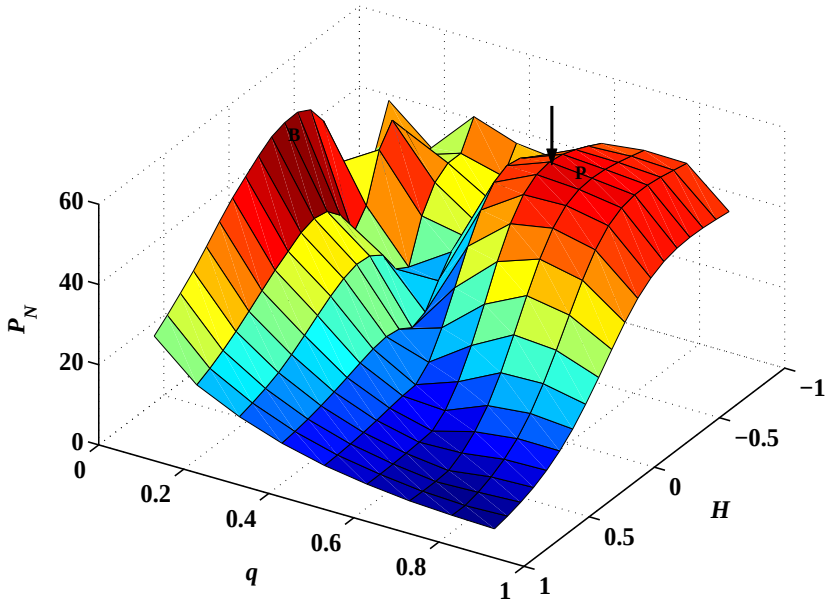

Figure 24: Dependence of the height $P_N(H, q)$ of the most significant peak in each Lomb periodogram of the (H, q)-derivative of the cumulative energy release before the rupture of tank $\#\,1$.

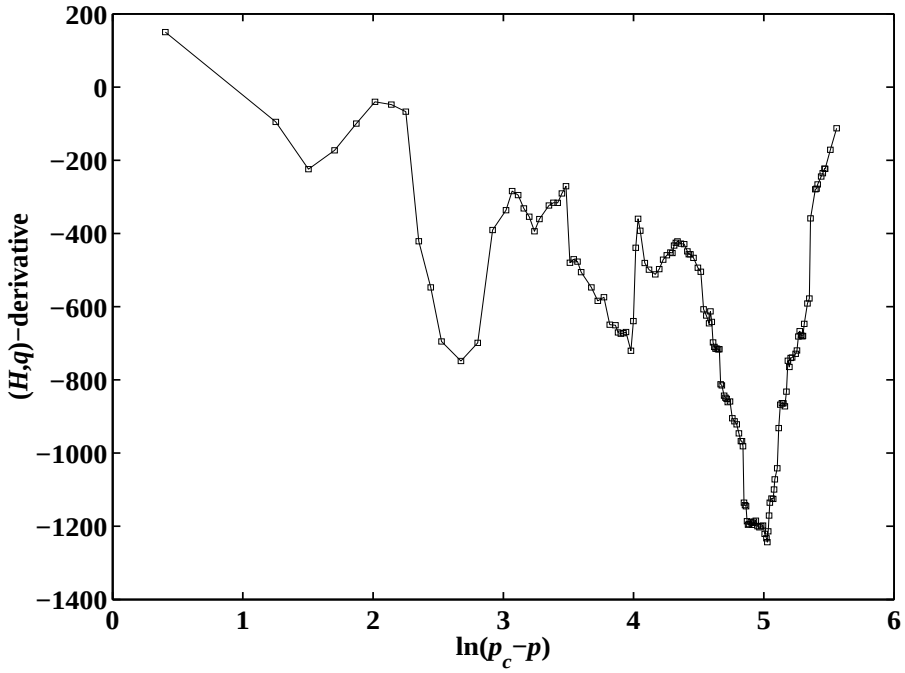

Figure 25: (H, q)-derivative of the cumulative energy release before the rupture of tank $\#1$ as a function of the pressure-to-rupture $p_c - p$ with $q = 0.6$ and $H = -0.5$.

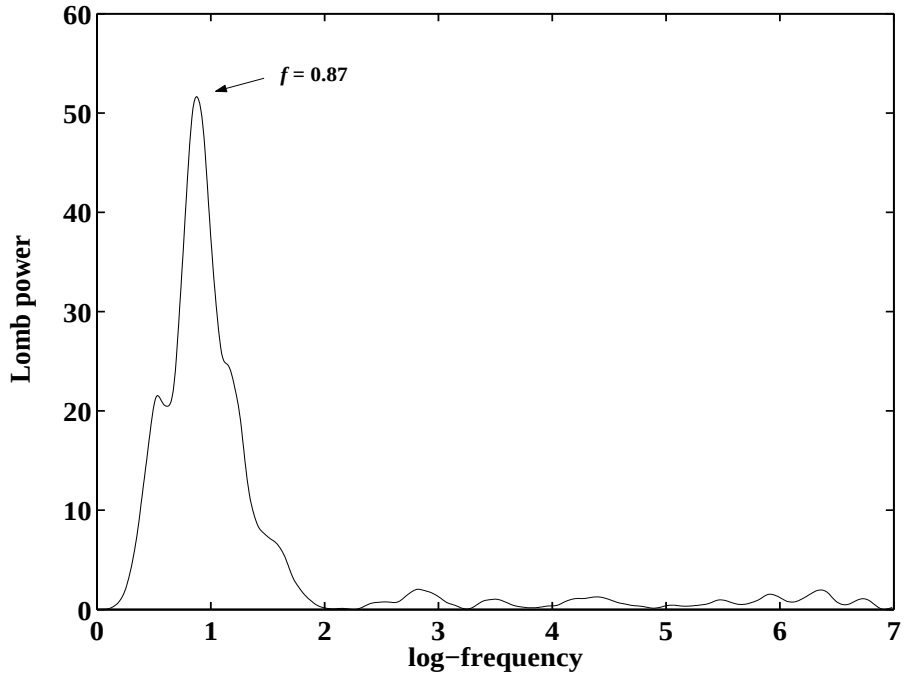

Figure 26: Lomb power of the (H, q)-derivative shown in Fig. 25.

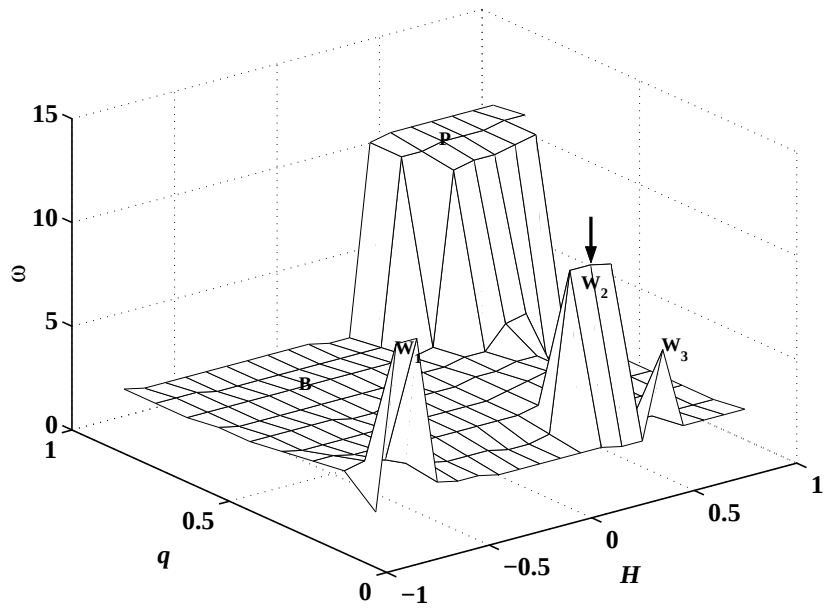

Figure 27: Dependence of the logarithmic angular frequency $\omega(H, q)$ of the most significant peak in each Lomb periodogram of the (H, q)-derivative of the cumulative energy release before the rupture of tank $\#\,2$.

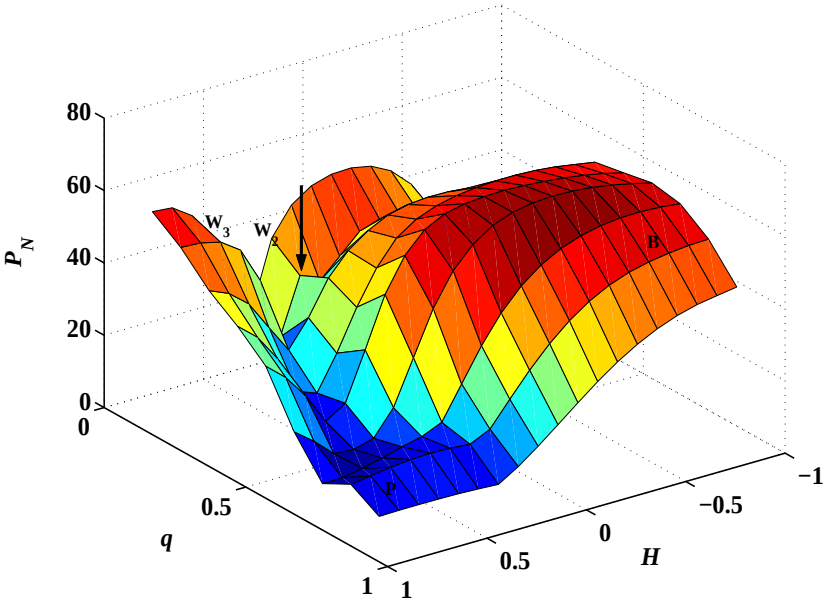

Figure 28: Dependence of the height $P_N(H, q)$ of the most significant peak in each Lomb periodogram of the (H, q)-derivative of the cumulative energy release before the rupture of tank $\#\,2$.

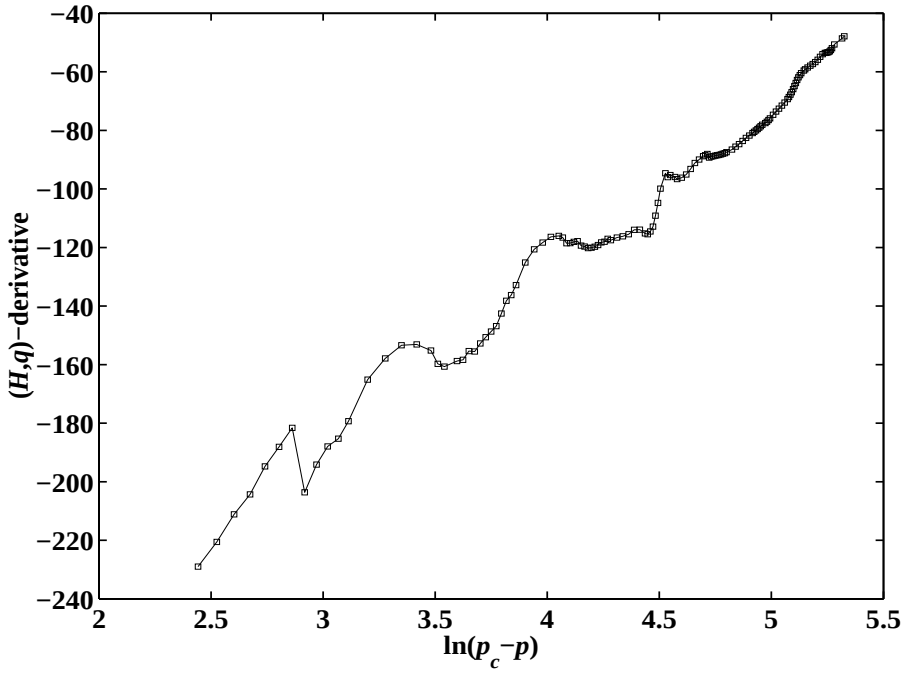

Figure 29: (H, q)-derivative of the cumulative energy release before the rupture of tank $\#\,2$ as a function of the pressure-to-rupture $p_c - p$ with $q = 0.2$ and $H = 0.3$.

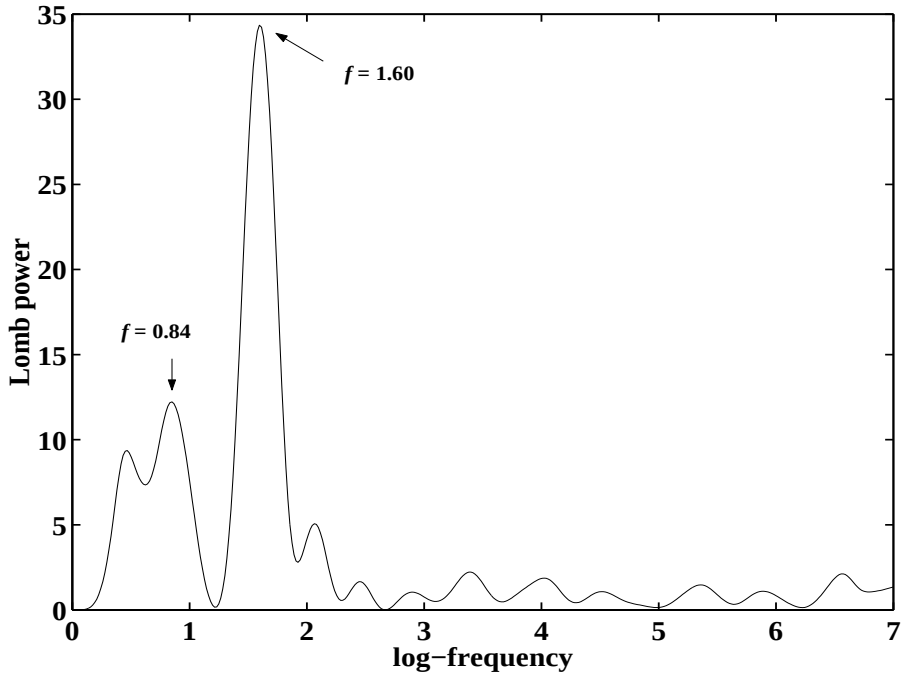

Figure 30: Lomb power of the (H, q)-derivative shown in Fig. 29. The fundamental log-frequency $f = 0.84$ and its harmonic $f = 1.60$ are indicated by arrows.

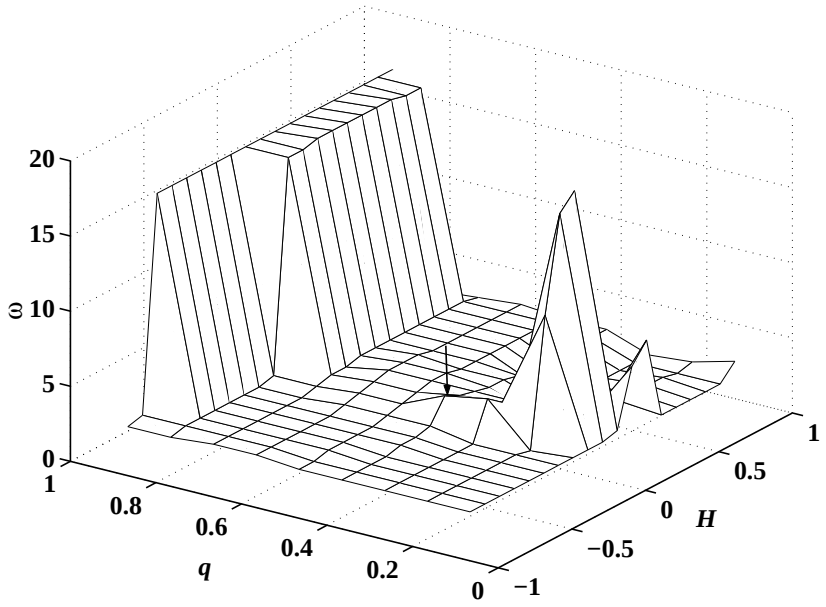

Figure 31: Dependence of the logarithmic angular frequency $\omega(H, q)$ of the most significant peak in each Lomb periodogram of the (H, q)-derivative of the cumulative energy release before the rupture of tank $\#\,3$. There are two wedges at $q \sim 0.1$ and 0.2 excluded according to the fourth criterion, around which is the bottom of a basin. The platform with $\omega > 15$ is excluded according to third criterion. The optimal pair $(-0.2, 0.4)$ is located within the second platform $[-0.2, 0.9] \times [0.4, 0.7]$.

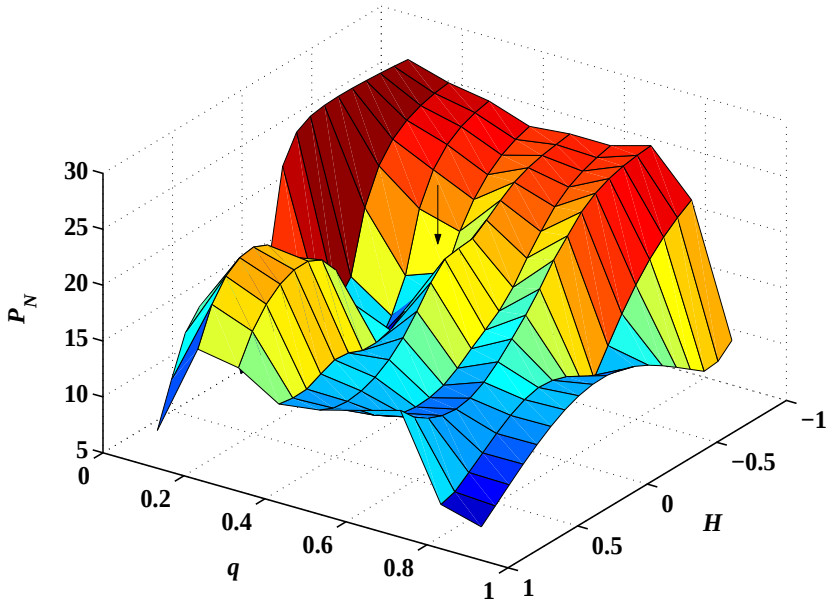

Figure 32: Dependence of the height $P_N(H, q)$ of the most significant peak in each Lomb periodogram of the (H, q)-derivative of the cumulative energy release before the rupture of tank $\#\,3$.

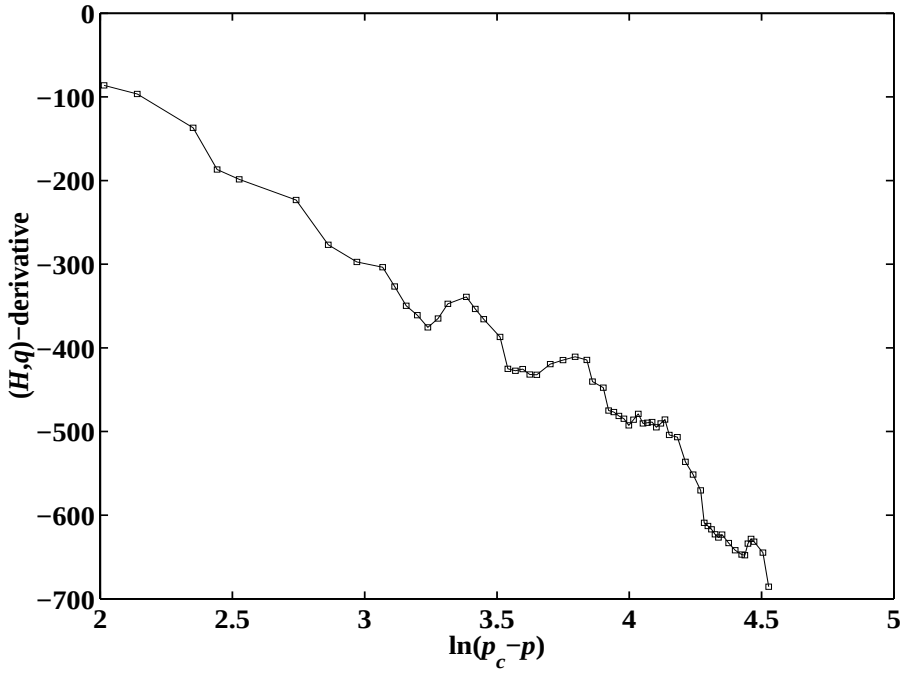

Figure 33: (H, q)-derivative of the cumulative energy release before the rupture of tank $\#\,3$ as a function of the pressure-to-rupture $p_c - p$ with $q = 0.4$ and $H = -0.2$.

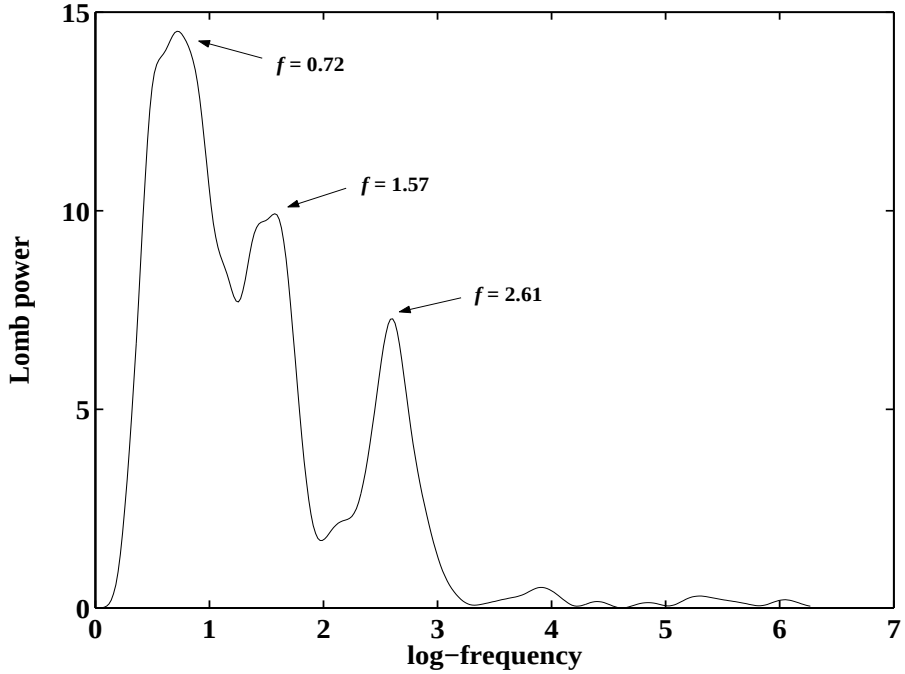

Figure 34: Lomb power of the (H, q)-derivative shown in Fig. 33. The logarithmic frequencies of the three highest peaks are $0.72, 1.57$ and 2.61, respectively.

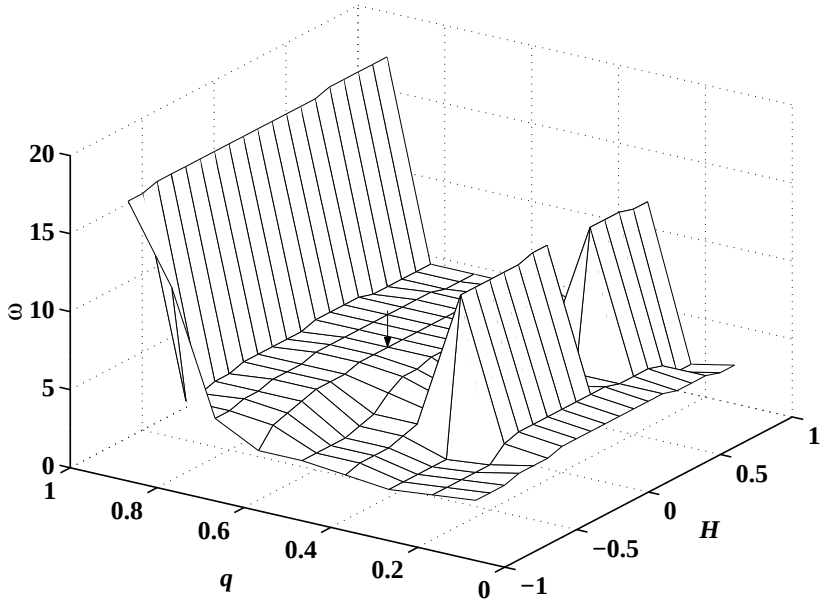

Figure 35: Dependence of the logarithmic angular frequency $\omega(H, q)$ of the most significant peak in each Lomb periodogram of the (H, q)-derivative of the cumulative energy release before the rupture of tank $\#\,4$. There are two wedges at $q = 0.3$ excluded according to the fourth criterion. The "wall" with $\omega > 15$ is excluded according to third criterion. The optimal pair $(0, 0.6)$ is located within the platform indicated by an arrow.

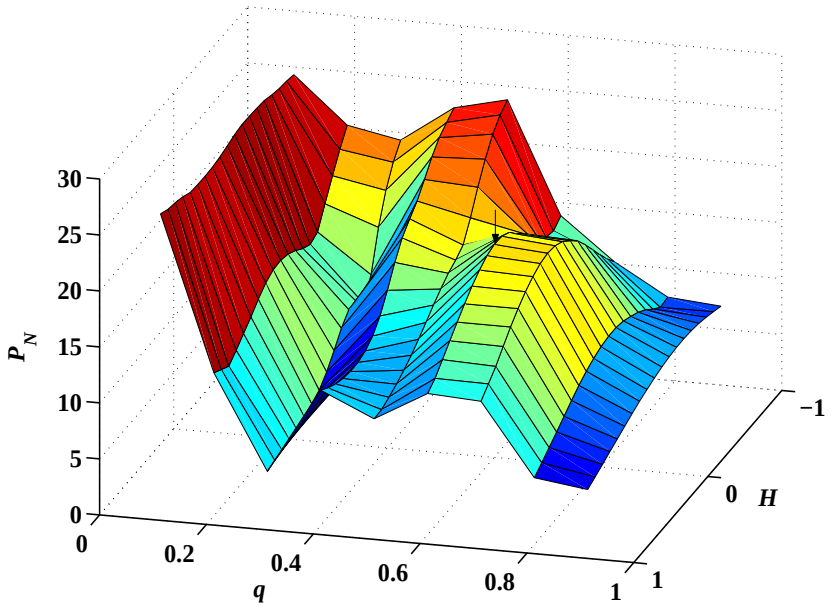

Figure 36: Dependence of the height $P_N(H, q)$ of the most significant peak in each Lomb periodogram of the (H, q)-derivative of the cumulative energy release before the rupture of tank $\#\,4$. The optimal pair $(0, 0.6)$ is indicated by an arrow.

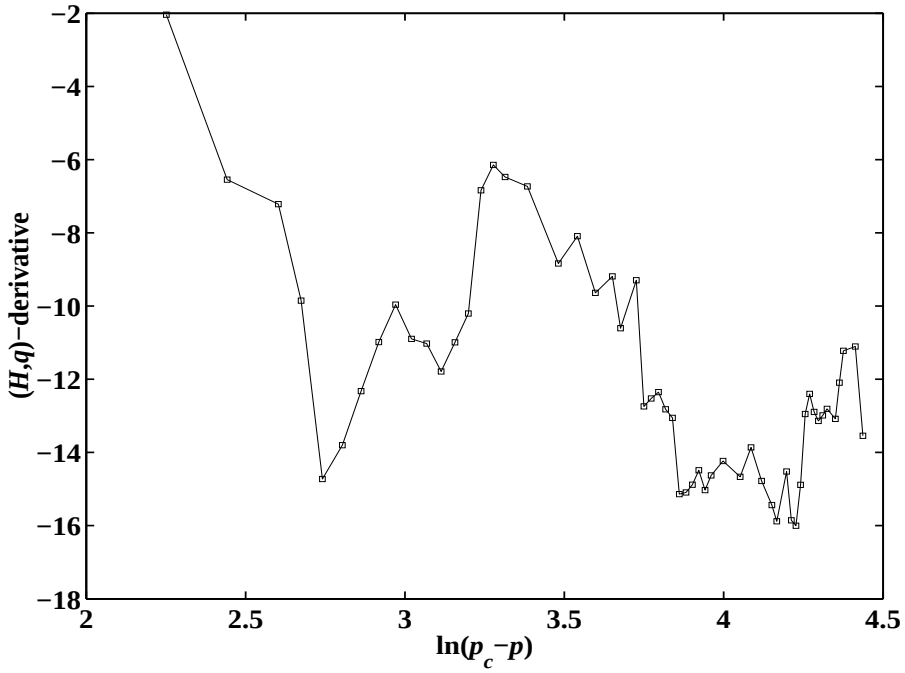

Figure 37: (H, q)-derivative of the cumulative energy release before the rupture of tank $\#\,4$ with respect to the pressure-to-rupture $p_c - p$ with $q = 0.6$ and $H = 0$.

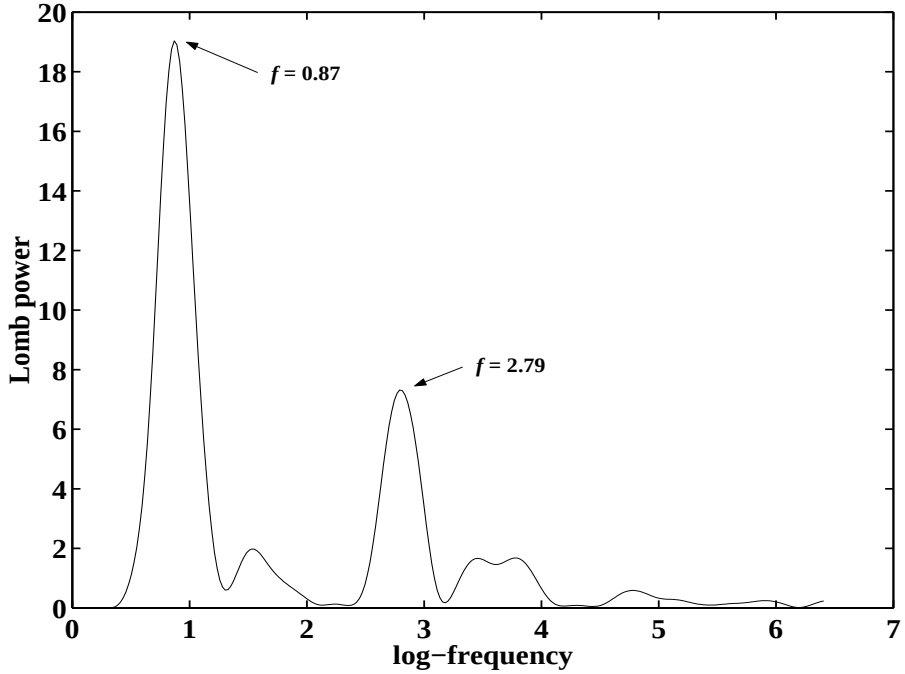

Figure 38: Lomb power of the (H, q)-derivative shown in Fig. 37. The logarithmic frequencies of the two highest peaks are 0.87 and 2.79, respectively.

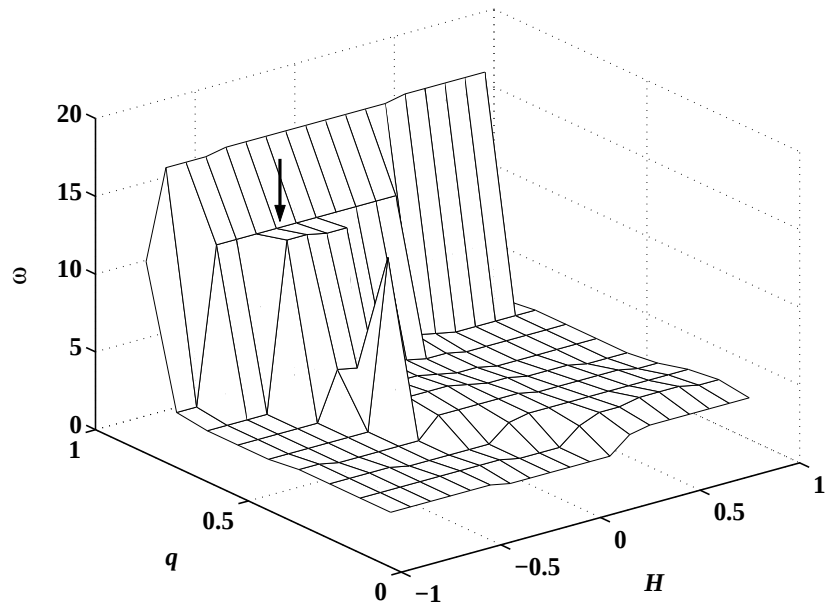

Figure 39: Dependence of the logarithmic angular frequency $\omega(H, q)$ of the most significant peak in each Lomb periodogram of the (H, q)-derivative of the cumulative energy release before the rupture of tank $\#\,6$. The optimal pair $(-0.3, 0.8)$ is located within a platform.

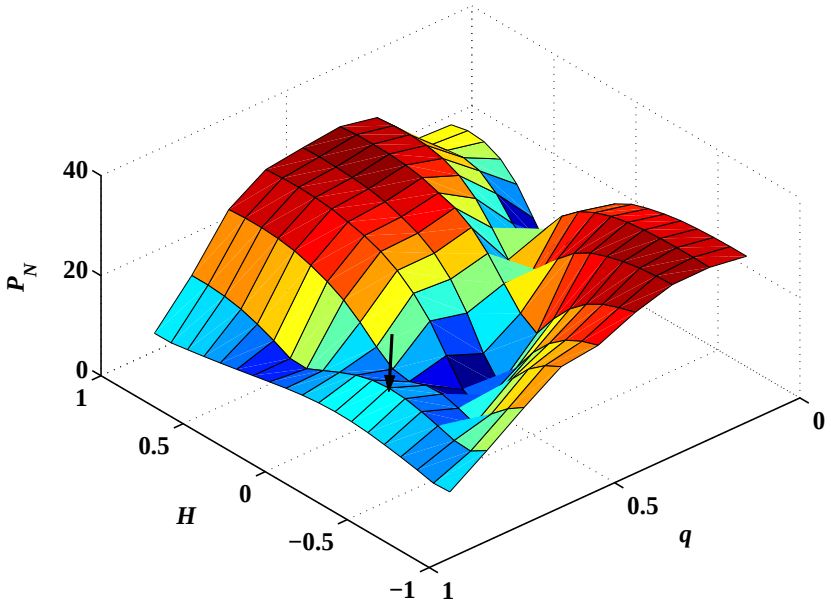

Figure 40: Dependence of the height $P_N(H, q)$ of the most significant peak in each Lomb periodogram of the (H, q)-derivative of the cumulative energy release before the rupture of tank $\#\,6$. The optimal pair $(-0.3, 0.8)$ is indicated by an arrow.

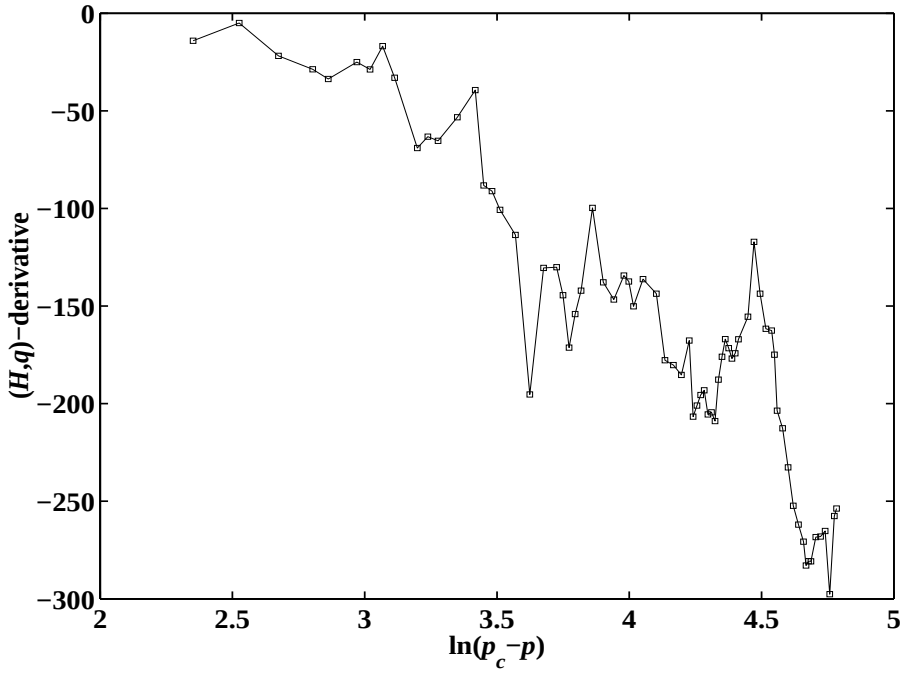

Figure 41: (H, q)-derivative of the cumulative energy release before the rupture of tank $\#\,6$ as a function of the pressure-to-rupture $p_c - p$ with $q = 0.8$ and $H = -0.3$.

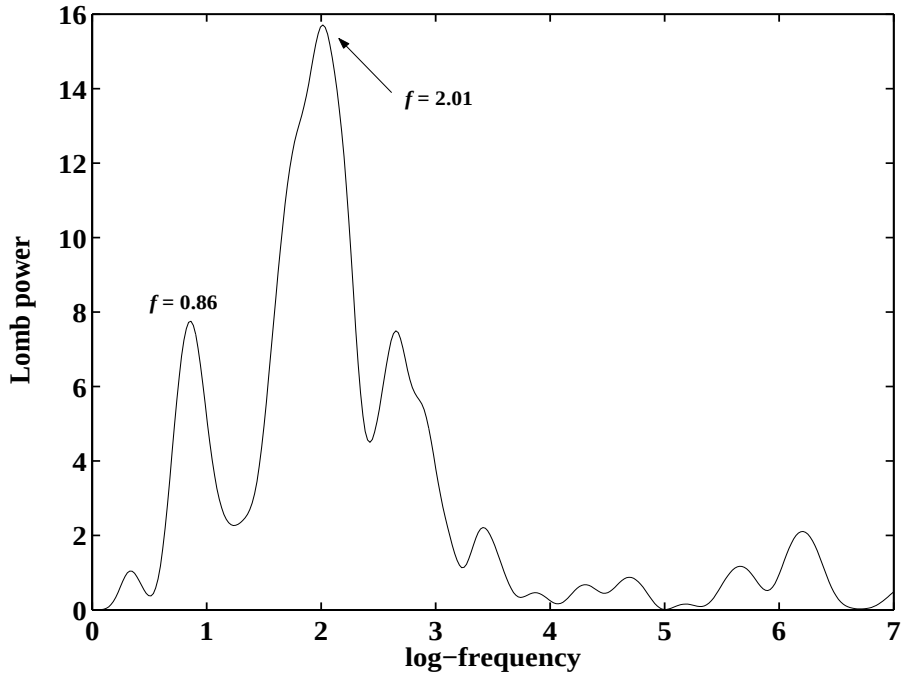

Figure 42: Lomb power of the (H, q)-derivative shown in Fig. 41. The fundamental log-frequency $f = 0.86$ and its harmonic $f = 2.01$ are indicated by arrows.

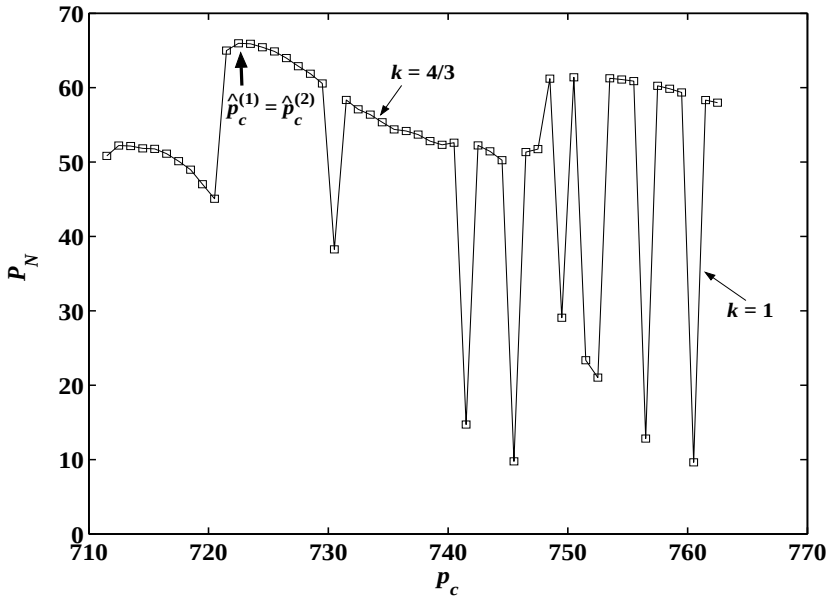

Figure 43: Post-diction of the critical pressure of the rupture of tank $\#1$. The two fine arrows indicate the upper threshold of predictable $\hat{p}_c$ estimated by Eq. (16) with $k = 4/3$ and $k = 1$. The coarse arrows indicate the predicted critical pressures $\hat{p}_c^{(1)}$, $\hat{p}_c^{(2)}$ and $\hat{p}_c^{(3)}$.

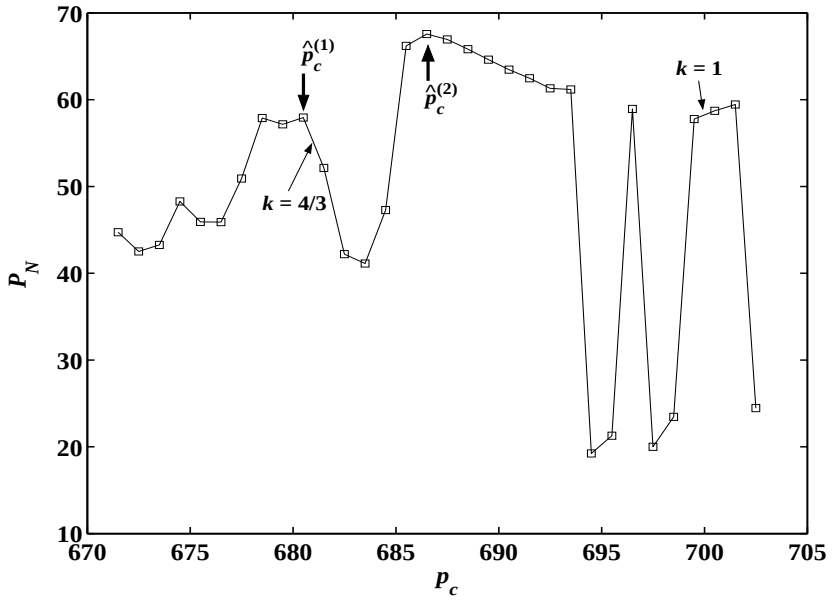

Figure 44: Post-diction of the critical pressure of the rupture of tank $\#2$. Same as in figure 43.

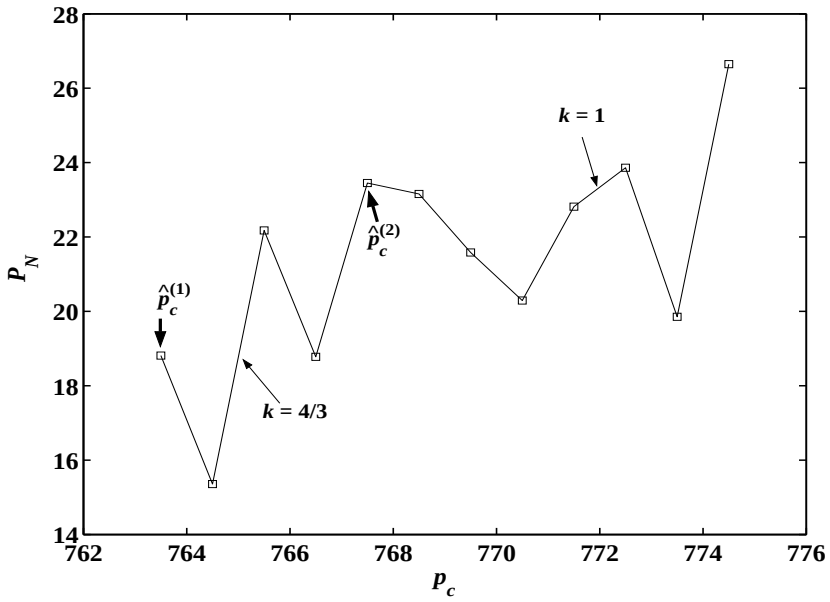

Figure 45: Post-diction of the critical pressure of the rupture of tank # 3. Same as in figure 43.

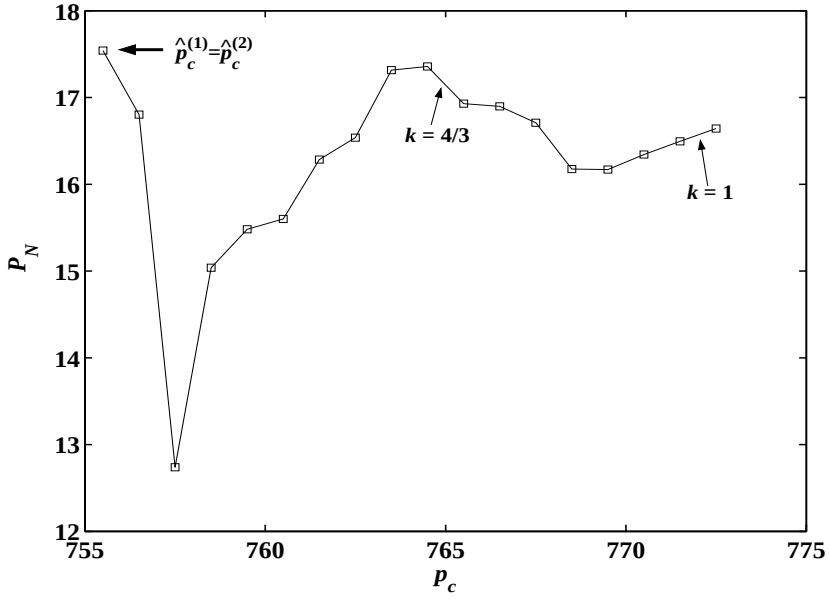

Figure 46: Post-diction of the critical pressure of the rupture of tank # 4. Same as in figure 43.

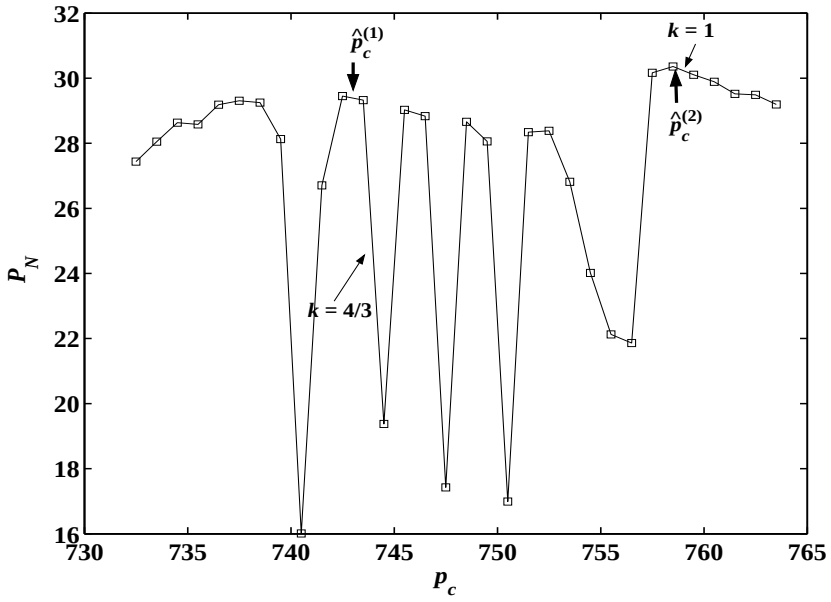

Figure 47: Post-diction of the critical pressure of the rupture of tank # 6. Same as in figure 43.